Serotonin sensing by microglia conditions the proper development of neuronal circuits and of social and adaptive skills

Giulia Albertini, Ivana D'andrea, Mélanie Druart, Catherine Béchade, Nayadoleni Nieves-Rivera, Fanny Etienne, Corentin Le Magueresse, Alexandra Rebsam, Nicolas Heck, Luc Maroteaux, et al.

Serotonin sensing by microglia conditions the proper development of neuronal circuits and of social and adaptive skills

Giulia Albertini[1,#], Ivana D'Andrea[1,#], Mélanie Druart[1], Catherine Béchade[1], Nayadoleni Nieves-Rivera[1], Fanny Etienne[1], Corentin Le Magueresse[1], Alexandra Rebsam[1,2], Nicolas Heck[3], Luc Maroteaux[1,*], Anne Roumier[1,*,✉]

[1] Sorbonne université, INSERM, Institut du Fer à Moulin, F-75005, Paris, France

[2] Sorbonne Université, INSERM, CNRS, Institut de la Vision, F-75012 Paris, France

[3] Sorbonne Université, CNRS, INSERM, Neurosciences Paris Seine, Institut de Biologie Paris Seine, F-75005, Paris, France

[#] These authors contributed equally: Giulia Albertini, Ivana D'Andrea

[*] These authors contributed equally: Luc Maroteaux, Anne Roumier

[✉] Corresponding author. Email: anne.roumier@inserm.fr

Abstract

The proper maturation of emotional and sensory circuits requires fine tuning of serotonin (5-HT) level during early postnatal development. Consistently, dysfunctions of the serotonergic system have been associated with neurodevelopmental psychiatric diseases, including autism spectrum disorders (ASD). However, the mechanisms underlying the developmental effects of 5-HT remain partially unknown, one obstacle being the action of 5-HT on different cell types.

Here, we focused on microglia, which play a role in brain wiring refinement, and we investigated whether the control of these cells by 5-HT is relevant for neurodevelopment and spontaneous behaviors in mice. Since the main 5-HT sensor in microglia is the 5-HT_{2B} receptor subtype, we prevented 5-HT signaling specifically in microglia by conditional invalidation of the *Htr2b* gene in these cells. We observed that abrogating the serotonergic control of microglia during early postnatal development affects the phagolysosomal compartment of these cells and their proximity to dendritic spines and perturbs neuronal circuits maturation. Furthermore, this early ablation of microglial 5-HT_{2B} receptors leads to adult hyperactivity in a novel environment and behavioral defects in sociability and flexibility. Importantly, we show that these behavioral alterations result from a developmental effect, since they are not observed when microglial *Htr2b* invalidation is induced later, at P30 onward.

Thus, a primary alteration of 5-HT sensing in microglia, during a critical time window between birth and P30, is sufficient to impair social and flexibility skills. This link between 5-HT and microglia may explain the association between serotonergic dysfunctions and behavioral traits like impaired sociability and inadaptability to novelty, which are prominent in psychiatric disorders such as ASD.

Introduction

Neurodevelopmental psychiatric disorders such as autism spectrum disorders (ASD) are characterized by alterations of spontaneous behaviors and personality traits, like social interactions and adaptability to novelty. Despite their high prevalence - roughly one percent of the total population for ASD -, preventive, diagnosis and therapeutic actions for these disorders are still limited by lack of understanding of their underlying pathophysiology. Among potential risk factors for neurodevelopmental psychiatric disorders are events or mutations that affect the immune system and notably the brain resident macrophages, microglia, which participate to neuronal migration, synapse formation and elimination [1]. An imbalance of the neuromodulator serotonin (5-HT) has also been incriminated [2–4]. Indeed, hyperserotonemia was one of the first biomarkers identified for autism [5] and is observed in 25% of ASD patients with current criteria [6]. Furthermore, 5-HT has developmental roles [7–9], and in mice, increasing or decreasing 5-HT availability during development, through genetic or pharmacological means, alters emotional and sensory neuronal circuits maturation, and has long-term effects on anxiety and sociability in adulthood [7–9]

The mechanisms underlying the implication of 5-HT in the etiology of neurodevelopmental disorders remain partly elusive due to the potential action of 5-HT on different cell types. Notably, besides neurons, which express a large array of serotonergic receptors, microglia express the 5-HT receptor subtype 2B (5-HT_{2B}) throughout postnatal life [10–12] and we have shown that 5-HT triggers a 5-HT_{2B}-dependent directional motility of microglial processes [10, 13]. In addition, *Htr2b*$^{-/-}$ mice, fully invalidated for the gene encoding 5-HT_{2B} receptors, show defects in the maturation of the retinal circuit in the thalamus [10], a developmental process of synapse elimination requiring both microglia and 5-HT [9, 14–16], and a wide spectrum of behavioral alterations [17]. However, the interpretation of *Htr2b*$^{-/-}$ mice phenotype is limited by the fact that *Htr2b* gene is expressed not only by microglia but also by subsets of serotonergic and dopaminergic neurons [18, 19]. Considering the prominent role of microglia in sculpting brain circuits, and their ability to respond to 5-HT, we tested here the hypothesis that impaired 5-HT sensing specifically in microglia is sufficient to alter the refinement of postnatal circuits, and thereby to induce alterations in spontaneous behaviors relevant to neurodevelopmental psychiatric disorders.

To this aim, using the tamoxifen-inducible creERT2/LoxP system in mice, we invalidated *Htr2b* gene specifically in the microglia/macrophage lineage, either just after birth, or after four weeks of postnatal development, a time point hereafter referred to as “P30”. Our results show that impairing 5-HT signaling in microglia since birth perturbs microglial development and the refinement of neuronal circuits, and leads to hyperactivity in a novel environment, poor sociability and limited behavioral flexibility. Importantly, such behavioral alterations are not induced by ablation of the microglial 5-HT_{2B} receptors after P30, demonstrating a developmental role of the serotonergic regulation of microglia for these spontaneous behaviors. Altogether, our results support the idea that 5-HT, via the 5-HT_{2B} receptor, controls microglia and some of their well-established effects on brain development, and that an early alteration of this serotonergic control can contribute to the etiology of neurodevelopmental disorders characterized by sociability and flexibility defects, such as ASD.

Results

1. Absence of 5-HT_{2B} receptors in neonatal microglia decreases their lysosome content, alters their morphology, and affects synapse-microglia proximity in the developing hippocampus.

During the first weeks of postnatal development, microglia proliferate and undergo morphological and functional maturation, with modifications in their phagocytic activity [20, 21]. A precise timing of these changes is necessary for microglia to properly regulate brain circuits formation through the induction of dendritic filopodia formation [22], engulfment of presynaptic elements [14, 23, 24], or promotion of spine maturation [25], but the determinants of this maturation are unknown. To investigate whether microglia development was affected by a lack of serotonergic sensing, we triggered an early postnatal ablation of microglial 5-HT_{2B} receptors by administrating tamoxifen to *Cx3cr1*$^{creERT2/+}$*;Htr2b*$^{fl/fl}$ pups between postnatal day (P)1 and P5 [12]. We then characterized microglia in these mice, named hereafter cKO_{birth}, at P15, in comparison with microglia in control cWT_{birth} mice of the same age, i.e., *Cx3cr1*$^{creERT2/+}$*;Htr2b*$^{+/+}$ mice similarly treated with tamoxifen at birth (timeline in **Fig. 1a**). Data from males and females were pooled except for parameters when a sex-dependent effect was observed (e.g., for morphology, see hereafter). First, we checked the microglial ($Iba1^+$ cells) density and did not detect effect of the genotype in any of the brain regions we analyzed (hippocampus, cortex, dorsal lateral geniculate nucleus (dLGN) of the thalamus) (**Fig. S1a-b**). Then, as developing microglia exhibit high phagocytic activity [23, 26, 27], we measured the percentage of microglial ($Iba1^+$) volume occupied by the macrophage phagolysosomal marker CD68. This revealed that the lysosomal content was strongly reduced (- 40%) in hippocampal microglia of P15 cKO_{birth} compared to cWT_{birth} mice (**Fig. 1b-c**). During postnatal development, microglia also undergo a transition from amoeboid to ramified [20, 21], in a sex-dependent manner [28]. We thus performed three-dimensional (3D) reconstructions of individual microglia in the hippocampus (*Cornu Ammonis* (CA) 1) at P15 (examples in **Fig. 1d**) to assess their morphology. In male mice, 3D Sholl analysis showed a reduced complexity of microglial processes in cKO_{birth} compared to cWT_{birth} (**Fig. 1e**), as well as a significant decrease in total length of processes and the number of processes terminal points (**Fig. 1f-g**). Noteworthy, these differences were not detected in females (**Fig. 1h-j**), showing a sex-dependent effect of 5-HT_{2B}-mediated signaling on microglia morphology at this age.

Physical contacts between microglia and dendritic spines participate to the sculpting of postnatal neuronal networks [22]. We thus analyzed the structural association of microglial processes with hippocampal dendritic spines. To do so, we performed DiI and P2Y12 receptor labeling to simultaneously visualize CA1 apical dendrites and microglia, and we measured the percentage of dendritic spines with microglial processes located within 0.3 µm of the spine head (scheme in **Fig. 1k** and representative images in **Fig. 1l**). By this approach, we determined that the proportion of spines in close proximity to microglia was reduced (- 30%) in cKO_{birth} mice (**Fig. 1m**). Of note, the probability for a spine to have a microglial process in its surroundings increases with its head diameter, and thus spine head size can be a confounding factor, but we verified that the proportion of spines apposed to a microglial process was reduced in cKO_{birth} mice whatever the spine head size (**Fig. S1c**). As this effect was observed despite unchanged microglia density, and both in males and females while the latter have a normal microglia morphology, it may indicate an intrinsic reduced ability of microglia to structurally interact with spines in the absence of 5-HT_{2B} receptor signaling.

In summary, ablation of 5-HT_{2B} receptor in microglia since birth perturbs microglial maturation at the structural and functional levels and decreases the contacts between dendritic spines and microglial processes during early postnatal development.

2. Absence of 5-HT_{2B} receptors in microglia since birth impairs brain wiring refinement in the developing hippocampus, cortex, and thalamus.

The first weeks of postnatal development are marked by intense synapse formation and pruning of connectivity, which enables the establishment of mature neuronal circuits. Microglia have been implicated in sculpting developing neuronal circuits postnatally through several mechanisms: removal of post- or presynaptic elements by engulfment-dependent [14, 22, 27] or -independent [29] mechanisms, or induction of dendritic protrusions growth [22, 30]. Having identified functional and structural defects in P15 microglia when their 5-HT sensing was disturbed, we investigated whether this may have affected connectivity at the same age (timeline **Fig. 2a**). We focused on hippocampus, cortex and thalamus, where the role of microglia in developmental axonal or synaptic refinement has been well documented [14, 24–27, 30]. Data from males and females were pooled after checking for the absence of sex-dependent effect.

In the hippocampus, we first used Golgi staining to analyze the morphology and density of protrusions, i.e., spines and filopodia-like spines, on the dendrites of CA1 pyramidal neurons (**Fig. 2b-e**). We observed that the density (**Fig. 2c**) and the length (**Fig. 2d**) of dendritic protrusions were increased in cKO_{birth} compared to cWT_{birth} mice. Accordingly, the distribution of protrusion types, as defined in [31], was significantly altered in cKO_{birth} mice (**Fig. 2e**). Of note, no differences in the spine head diameter were observed (**Fig. S1d**), further confirming no spine head-related bias in the spine-microglia proximity phenotype mentioned previously. Interestingly, similar alterations in protrusions density, length and types distribution were observed in the prefrontal cortex (L2/L3 principal neurons) (**Fig. S2a-e**). Second, to confirm functionally the existence of synaptic alterations in the hippocampus, we performed whole-cell electrophysiological recordings of CA1 pyramidal neurons on acute brain slices. Indeed, hippocampal neurons from cKO_{birth} P15 mice displayed higher miniature excitatory postsynaptic currents (mEPSCs) frequency compared to controls, despite no changes in amplitude (**Fig. 2f-h**). Thus, the early impairment of 5-HT sensing in microglia induces structural and functional synaptic alterations in the hippocampus and cortex, and thus impairs circuits maturation.

Another region undergoing prominent refinement soon after birth is the dLGN of the thalamus [14, 23, 24], where eye-specific segregation of retinal projections requires both appropriate 5-HT levels [32] and functional microglia [14]. We previously demonstrated that the maturation of this visual circuit is impaired in *Htr2b* full knock-out mice [10]. Here, the conditional knock-out model allowed us to test if the axonal refinement in the dLGN was dependent on the microglial 5-HT_{2B} receptor. We observed that ipsilateral and contralateral retinal inputs were actually significantly less segregated, i.e., more overlapped, in cKO_{birth} than in cWT_{birth} mice at P17-18 (**Fig. 2i-j**), a time point when segregation is normally achieved. Such defective axonal refinement was confirmed by the fact that ipsilateral projections in cKO_{birth} mice were scattered over a greater dLGN area than in cWT_{birth} mice (**Fig. S2f-h**).

Noteworthy, immunoreactivity for vGLUT1 in the hippocampus or vGLUT2 in the dLGN is found within the $CD68^+$ compartment of P15 microglia of both genotypes (**Fig. S3a-b**), confirming that microglia engulf presynaptic material in both regions, consistently with previous reports [14, 22, 26, 29, 33]. Moreover, the volume of vGLUT1/2 is linearly correlated to the size

of the phagolysosomal compartment (CD68 volume), and both are lower in cKO microglia of both regions, suggesting that microglia in cKO_{birth} mice have a general phagolysosomal defect rather than a specific deficiency in synaptic material removal (**Fig. S3c**).

Overall, our results in different brain areas demonstrate that impairment of 5-HT sensing in microglia since birth affects synaptic pruning, axonal refinement and thus brain wiring in the first weeks of postnatal development.

3. Absence of 5-HT_{2B} receptors in microglia since birth impacts activity of mice in a novel environment, sociability, and flexibility.

Alterations of brain development can be compensated with age or on the contrary lead to persistent behavioral deficits. To assess long-lasting consequences of interrupting 5-HT_{2B} receptor-mediated signaling in microglia since birth, we profiled the behavior of adult (or, for one test, juvenile) cKO_{birth} mice in three domains commonly altered in neurodevelopmental psychiatric disorders: (i) behavior in a novel environment; (ii) social skills; (iii) flexibility. All behavioral experiments were performed and analyzed separately on males (**Fig. 3**) and females (**Fig. 4**).

Significant alterations were observed in males (timeline in **Fig. 3a)**. Indeed, when adult cKO_{birth} male mice were exposed to a novel environment, they responded with significantly increased locomotion (**Fig. 3b**) compared to cWT_{birth} mice. This effect seemed to be due to the novelty of the environment rather than hyperactivity *per se*, being more prominent at the beginning of the test. Moreover, when placed in an unfamiliar cylinder, male cKO_{birth} mice spent significantly more time self-grooming than cWT_{birth} mice (**Fig. 3c**), suggesting an increased propensity to repetitive stereotypic behavior under unknown and stressful conditions. To identify early deficits in social behavior, we performed the maternal homing test (**Fig. 3d-f**) on juvenile mice. In the first configuration of the test (**Fig. 3d, upper panel**), juvenile cKO_{birth} male mice spent significantly more time in the corner with home cage bedding than with fresh bedding (**Fig. 3e**), demonstrating an intact ability to recognize familiar olfactory cues. However, in the second configuration where we introduced two mesh tubes, one empty and one containing the juvenile's mother (**Fig. 3d, lower panel**), the time spent in the corner containing the latter tube was significantly reduced, and the time spent in the corner containing the empty tube was increased, in cKO_{birth} mice compared to cWT_{birth} (**Fig. 3f**). The social deficit seen in cKO_{birth} juvenile mice toward their mother persisted in adulthood toward unfamiliar mice. Indeed, in a neutral territory, cKO_{birth} adult male mice spent less time interacting with an unfamiliar (wild type) juvenile compared to cWT_{birth} (**Fig. 3g**). We further explored the social skills of male mice by investigating their social flexibility. To this aim, we recorded the spontaneous social behavior in home cage of male mice housed with a familiar cage mate, during two consecutive days, using the change of litter bedding after day 1 to challenge the social hierarchy (**Fig. 3h**) [34]. cWT_{birth} mice adapted their behavior in response to this challenge, as expected: on day 2, they showed less social investigation than on day 1 when social hierarchies were defined (**Fig. 3i**). By contrast, cKO_{birth} mice behaved independently of the environmental challenge, spending similar time interacting with the conspecific on day 1 and on day 2 (**Fig. 3i**), and overall less time than the cWT, in accordance with their sociability deficit (assessed in **Fig. 3d-g**). The difference in social flexibility between cWT and cKO_{birth} mice was also illustrated by the increased aggressive behavior of cWT on day 2, while cKO_{birth} mice displayed an abnormal aggressive behavior overall (**Fig. 3j**). These results confirm a strong social impairment and reveal traits of social inflexibility in cKO_{birth} mice. To understand if the impairment in flexibility could be generalized beyond the social domain, we assessed cognitive flexibility with a reversal learning test (**Fig. 3k-l**). During the acquisition phase, cKO_{birth} male mice learned to choose the correct arm

of the Y-maze, containing a food reward, as rapidly as the cWT_{birth} mice. By contrast, in the reversal phase of the test, cKO_{birth} male mice failed to learn the new position of the correct arm (**Fig. 3l**), which shows that early invalidation of 5-HT_{2B} receptors in microglia decreases not only social but also cognitive flexibility.

Sex differences have been reported in many psychiatric disorders, with notably a higher prevalence of neurodevelopmental disorders in males [35]. We thus assessed whether cKO_{birth} females presented similar behavioral phenotypes than those observed in mutant males (timeline in **Fig. 4a**). When placed in a novel environment, adult cKO_{birth} female mice didn't show hyperlocomotion (**Fig. 4b**). Nonetheless, as mutant males, cKO_{birth} females showed enhanced self-grooming in an unfamiliar cylinder compared to cWT (**Fig. 4c**), suggesting an increased propensity to repetitive stereotypic behavior. We also observed a phenotype for juvenile cKO_{birth} female mice in the maternal homing test, similar as the one observed in cKO males: despite a normal preference for the nest corner *vs* empty corners (**Fig. 4d**), the time spent in the corner containing the tube containing their mother was significantly reduced, and the time spent interacting with the empty tube and in the empty corner were increased, compared to cWT_{birth} females (**Fig. 4e**). We did not observe defects in social behavior in adult females (**Fig. 4f**), which might be due to the different nature of social activity between the two sexes at adulthood, male mice being more sensitive to environmental modifications and more prone to increase their repertoire of social explorations to assess social hierarchy [36]. Finally, we assessed cognitive flexibility with the reversal learning test. As observed for mutant males, after a normal acquisition phase, cKO_{birth} females failed to learn the new position of the correct arm in the reversal phase, in comparison with the cWT_{birth} females (**Fig. 4g)**. Of note, since most behaviors required intact olfactory capacities, we tested both genotypes in the olfactory habituation/dishabituation test, and we did not detect any difference in their olfactory skills (males: **Fig. S4a**, females: **Fig. S4b**).

Overall, early invalidation of *Htr2b* in microglia leads to severe behavioral alterations in both sexes. The phenotype is however particularly pronounced in males, where it is characterized by increased activity (locomotion, self-grooming) in a novel environment, decreased sociability, and deficits in social and cognitive flexibility. These defects could be linked to the early microglial and synaptic alterations observed in cKO_{birth} males and females at P15. However, given the importance of 5-HT in adult behavior, and the expression of 5-HT_{2B} receptor gene in microglia throughout life, we performed additional experiments to disentangle the developmental versus adult (acute) effects of 5-HT signaling in microglia on the phenotype observed.

4. Ablation of 5-HT_{2B} receptors in microglia at P30 does not alter spontaneous behaviors.

To test a possible adult/acute role of serotonin to microglia signaling in the behavioral alterations observed in cKO_{birth} adult mice, we repeated the same behavioral tests on mice where invalidation of microglial *Htr2b* gene had been induced only after four weeks of postnatal life ("P30"), i.e. once microglia are mature and synaptogenesis and pruning completed [1]. To this aim, $Cx3cr1^{creERT2/+};Htr2b^{fl/fl}$ mice, as well as control $Cx3cr1^{creERT2/+};Htr2b^{+/+}$ mice, were treated with a first dose of tamoxifen between P28 and P30 and a second one 48h later, to generate cKO_{P30} and cWT_{P30} mice, respectively. This protocol was previously shown to be as efficient as the early tamoxifen treatment to induce recombination at the *Htr2b* locus (Fig. S7 in [12]). Behavioral experiments were performed at least one month after tamoxifen treatment (timeline: **Fig. 5a**), and males and females were analyzed separately (in **Fig. 5** and **S5**, respectively). In this late ablation condition, after checking normal olfactory skills (males: **Fig. S4c**; females: **Fig. S4d**), we did not detect any deficit in locomotion or self-grooming in a new environment (males: **Fig. 5b-c**; females:

Fig. S5a-b), nor in sociability (males: **Fig. 5d**; females: **Fig. S5c**), or in social (males: **Fig. 5e-f**) or cognitive flexibility (males: **Fig. 5g**; females: **Fig. S5d**). This is consistent with the idea that these behavioral domains rely on the establishment of a proper brain connectivity during early postnatal development [37]. Besides, these results indicate that the behavioral defects observed when microglial *Htr2b* is invalidated since birth are directly linked to an impairment of serotonergic signaling to microglia during a postnatal window between birth and P30.

Discussion

In this work, our aim was to investigate if disturbed sensing of 5-HT by microglia affects microglial and neuronal maturation and can be implicated in behavioral alterations observed in neurodevelopmental psychiatric disorders. Our findings prove that interrupting the serotonergic control of microglia perturbs microglial functions during postnatal development, affects synaptic and axonal refinement in several brain regions at P15-P18, and induces long-lasting behavioral phenotypes in adulthood such as repetitive behavior in a new environment, deficits in sociability and a lack of behavioral flexibility. Importantly, these behavioral alterations, which are reminiscent of core symptoms of neurodevelopmental disorders, are not induced by the ablation of microglial 5-HT_{2B} receptors after P30. This work thus provide evidence that behavioral features (including response to novelty, sociability, and flexibility) require the developmental control of 5-HT on microglia.

Microglial 5-HT_{2B} receptor is required in the neonatal period for proper microglial functions and brain wiring. Our data demonstrate that early (i.e., since birth) invalidation of microglial *Htr2b* triggers higher density of dendritic spines and enhanced excitatory neurotransmission in the hippocampus at P15, indicating a defect in circuits maturation. Besides, in the dLGN, presynaptic contralateral and ipsilateral inputs are still intermingled at P18 in cKO_{birth} mice, indicating a delay in circuit refinement in the thalamus too. We thus propose that the lack of instruction by 5-HT induces a global defect in microglia maturation and function, which impairs their ability to shape neuronal circuits in different brain regions. The precise mechanisms by which the defects occur in cKO_{birth} mice will warrant further investigation, but some leads can be suggested. Microglia can contribute to circuit refinement through the engulfment of presynaptic structures [14, 22–24] or through active contacts with dendrites promoting spines formation or remodeling [22, 30]. Here, the density of microglia in cKO_{birth} mice at P15 is normal in all the regions we examined, but in the hippocampus, cKO_{birth} microglia display reduced $CD68^+$ phagolysosomal volume at P15 and this compartment contains presynaptic material. The same tendency is observed in the dLGN of the thalamus. Moreover, the phagolysosomal volume of microglia is correlated to their content in presynaptic material. A global reduction in phagocytosis could thus explain at least in part the increased connectivity in hippocampus and the lack of axonal segregation in the thalamus. However, other mechanisms could be involved, such as altered levels of secreted or membrane factors regulating synapse stability [29, 38] or neuronal activity [39, 40]. Noteworthy, we also discovered that in the hippocampus, a reduced fraction of spines is found in close proximity of microglial processes in cKO_{birth} mice. Such reduced proximity could also contribute to the enhanced excitatory neurotransmission observed, given that microglia are able to provide a negative feedback control of spine activity [41].

Microglial 5-HT_{2B} receptor supports the serotonin-dependent refinement of the visual thalamus during postnatal development. It was previously reported that segregation of retinal projection into eye-specific territories in the dLGN does not occur in monoamine oxidase A knock-out mice (MAOA-KO), which have elevated brain levels of 5-HT, and that these defects can be

reversed by inhibiting 5-HT synthesis from P0 to P15. The serotonin transporter (SERT), which is transiently expressed in the dLGN into the ipsilateral retinal projection fields, has been proposed to confer specific neurotransmission properties on a subset of retinal ganglion cells that are important for proper segregation of retinal projections [15]. This was reinforced by the complementary evidence that eye-specific segregation in the dLGN and topographic refinement of ipsilateral axons in the dLGN are impaired in mice lacking vesicular release, in RIM1/2 conditional knock-out mice in SERT-positive neurons [42]. We previously reported that full 5-HT_{2B} receptor deficiency induces anatomical alterations of the ipsilateral projecting area of retinal axons into the dLGN at P30, validating the contribution of this receptor into 5-HT-dependent retinal projection segregation [10]. Here, we demonstrate that presynaptic contralateral and ipsilateral inputs in the dLGN are still intermingled in cKO_{birth} mice at P17-18, revealing that part of the 5-HT contribution to this segregation is to control microglia. Regarding the mechanism, it has been well described that microglia contribute to refinement in this region through phagocytosis of axons [14], and we find presynaptic material inside thalamic microglia, but less in cKO_{birth} than in cWT_{birth}. As discussed above, a general alteration of the phagocytic ability of cKO_{birth} microglia is likely to contribute to the segregation defect seen in the dLGN, but other mechanisms regulating synapse formation and turnover could be involved.

Microglial 5-HT_{2B} receptor is required during the neonatal period, but not later, for adult social behavior and cognitive flexibility. We previously reported defects in social interactions in *Htr2b*$^{-/-}$ male mice [17]. Hereby, we observed that, if microglial 5-HT_{2B} receptors are absent since birth, both male and female mice later display a plethora of behavioral abnormalities resembling key symptoms of neurodevelopmental psychiatric disorders, notably abnormal response to novelty, and decreased sociability and adaptability. Intriguingly, these behavioral alterations were not induced by the absence of these receptors after P30. This suggests that 5-HT acts as a global modulator of microglia during the critical time-window of postnatal development between birth and P30, which is required for the establishment of specific behavioral domains.

Sex-dependent effects of the invalidation of microglial 5-HT_{2B} receptors. Microglia exhibit sexually dimorphic transcriptomic and morphological differences along postnatal development and adulthood [28, 43–45]. Since neurodevelopmental and psychiatric disorders show a marked sexual dimorphism, it is plausible that sex-dependent microglial functions contribute to the different prevalence of these diseases among males and females. As well, a PET scan study demonstrated that women's brains show lower 5-HT activity [46], possibly reflecting a sex-dependent contribution of 5-HT to psychiatric disorders. We therefore paid attention to possible sex-dependent effects of microglial 5-HT_{2B} receptors invalidation and observed indeed that early invalidation of microglial *Htr2b* induces a significant alteration of the microglial morphology (reduced complexity of the ramifications) in male mice only. However, the other effects of the early invalidation of microglial 5-HT_{2B} receptors (impairment of microglial CD68 content, synaptic refinement, behavior), were observed in both sexes, which highlights the universal importance of 5-HT sensing by microglia during postnatal development.

Mechanisms linking activation of microglial 5-HT_{2B} receptors and downstream effects. A still open question concerns the intracellular signaling effectors of 5-HT in microglia. Both 5-HT and ATP/ADP, activating P2Y12 receptors, induce directional motility of microglial processes [10, 13, 47]. Moreover, pharmacologic or genetic P2Y12 receptors disruption in adolescent mice induces a reduction in microglial ramification [48], similar to what we observed

in males mice invalidated for *Htr2b*. It is thus possible that G_q-coupled 5-HT_{2B} and G_i-coupled P2Y12-receptor-mediated signals are interconnected, either physically, as GPCR heterodimers [49], or functionally. This latter possibility would remind of a mechanism existing in platelets, where shape changes are induced either by ADP [50] or 5-HT [51] through activation of P2Y12 or 5-HT_{2A} – which is structurally very close to 5-HT_{2B} – receptors, respectively, and inhibited by P2Y12 or 5-HT_{2A} receptor antagonists [52, 53]. Our results also raise the question of how the stimulation of microglial 5-HT_{2B} receptors affects on synapses and neurons. Considering the effects of 5-HT on microglial processes and on platelets, it is possible that in a wild-type context, activation of 5-HT_{2B} receptors on microglia regulates acutely their adhesion properties and their cytoskeleton, and thus their motility, intracellular trafficking, and secretion of factors. It could also control the expression of genes underlying microglial functional maturation. Disturbance of any of these regulations in the absence of 5-HT_{2B} receptors could challenge the interaction of microglia with neurons, axons, dendrites and thereby their capacity to support neuronal networks refinement.

In summary, our data strongly support that 5-HT acts as an upstream global modulator of microglial functions during early postnatal development, and that a lack of serotonergic control of microglia affects brain connectivity refinement and thereby a variety of behaviors that are altered in neurodevelopmental disorders. Given the number of exogenous factors known to change 5-HT levels during postnatal development, such as physical abuse, maternal separation and maternal inflammation, stress, antidepressants, and their correlation to neurodevelopmental disorders, our findings further emphasize the need of optimal brain levels of 5-HT for proper brain development and function throughout life. Besides, as the serotonergic system is targeted by an array of pharmacological compounds, this newly identified pathway of microglia regulation might open new therapeutic avenues for early intervention in neurodevelopmental disorders.

Materials and methods

Animals

Animal experiments were carried out according to the national guidelines on animal experimentation and were approved by the Ethical Committee for Animal Experiments of the Sorbonne University, Charles Darwin C2EA - 05 (authorization N°APAFIS#28230-2020111619109364 v4, and 01170.02). All efforts were made to minimize animal suffering. Results are described in accordance with the ARRIVE guidelines for reports in animal research [54]. To obtain targeted invalidation of *Htr2b* gene in microglia, we crossed the *Cx3cr1*^{creERT2} line (MGI Cat# 5528845, RRID:MGI:5528845), which express a tamoxifen-activable cre recombinase under the control of the endogenous *Cx3cr1* promoter, and the *Htr2b*^{flox} line (*Htr2b*^{tm2Lum}*/Htr2b*^{tm2Lum}*, IMSR Cat# EM:05939,* RRID:IMSR_EM:05939), where loxP sites are inserted around the first coding exon of *Htr2b* gene, allowing invalidation of the gene when the recombinase is activated by tamoxifen as previously described [12, 38, 55]. All lines were backcrossed on 129S2 background for more than 10 generations. *Cx3cr1*$^{creERT2/+}$*;Htr2b*$^{fl/fl}$ mice were used to obtain the conditional invalidation (see below the protocol to activate the creERT2 recombinase with tamoxifen). *Cx3cr1*$^{creERT2/+}$*;Htr2b*$^{+/+}$ mice, similarly, treated with tamoxifen, were used as control mice. P15, P25 or P80-120 male and female animals were used for the experiments (experimental design summarized in **Table 1**). As shown along the Results, Figures and Legends, data from males and females are presented separately for microglia morphology and for behavioral experiments, and pooled when no sex-dependent effect was apparent. All mice were

group-housed (2–5 mice per cage) in a 12/12 h light/dark cycle with free access to food and water. Temperature and relative humidity were kept at 21±1°C and between 30% and 60%, respectively.

Tamoxifen administration

To study the consequences of invalidation of microglial *Htr2b* at different time points, we used the following experimental approaches. First, to invalidate the *Htr2b* gene since birth ("early" invalidation), we performed intragastric administrations of 50 µg of tamoxifen (Sigma-Aldrich, T5648) per day for 3 days between P1 and P5 as previously described [56] giving rise to cKO_{birth} and cWT_{birth} mice. In a second approach, to invalidate the *Htr2b* gene since P30 ("late" invalidation), tamoxifen was administrated twice between P28 and P32, at 48 h interval, via oral gavage (each gavage corresponding to 0.2 mg tamoxifen.g^{-1} body weight), as previously described [38] giving rise to cKO_{P30} and cWT_{P30} mice. Of note, we previously validated the efficacy of these protocols to activate creERT2 recombinase by determining by qPCR the level of *Htr2b* recombination in the microglial fraction of mice that received early or late tamoxifen administration, demonstrating a similar decrease (>85%, Figure S7C in [12]). Moreover, we waited at least 1 month after tamoxifen treatment to allow the full renewal of peripheral $Cx3cr1^+$ cells [38, 57–60].

Immunohistochemistry

Mice were deeply sedated (pentobarbital, 140 mg.kg^{-1} i.p.) and transcardially perfused with 4% formaldehyde in 0.1 M phosphate buffered saline (PBS). Brains were harvested and immersed in the same fixative for 24 h at 4°C. Afterwards, they were transferred to a PBS solution with 0.01% sodium azide until being cut. 50 µm-thick coronal slices were cut using a vibratome (Leica). Brain slices covering the regions of interest were selected following the mouse brain atlas of Franklin and Paxinos [61]. Brain slices were washed one time in PBS, then incubated in permeabilizing and blocking solution (0.25% gelatin and 0.1% triton in PB) for 30 min. Primary antibodies, rabbit anti-Iba1 (0.0013 µg.$µL^{-1}$, Wako 019-19741), rat anti-CD68 (0.002 µg.$µL^{-1}$, AbD Serotec MCA1957) and rat anti-P2Y12 receptor (0.5 µg.$µL^{-}$1, Biolegend 848002), were diluted in PGT buffer (0.125% gelatin and 0.1% triton in PB). Samples were incubated for 24 h at 4°C with gentle agitation. After rinsing three times with PGT 0.125% buffer, secondary fluorochrome-conjugated antibodies were added to PGT buffer for 3h at room temperature. To quantify $Iba1^+$ cells density, we used a donkey anti-rabbit Cy3 (0.002 µg.$µL^{-1}$, Jackson Laboratories 711-165-152); to colocalize Iba1/CD68 and to assess $Iba1^+$ cells morphology, we used donkey anti-rabbit 488 (0.002 µg.$µL^{-1}$, Invitrogen A21206) and donkey anti-rat Cy3 (0.002 µg.$µL^{-1}$, Millipore AP189C). After rinsing three times with PGT 0.125% buffer and once with PBS, sections were mounted in Mowiol containing DAPI (0.005 µg.$µL^{-1}$, Sigma).

Image acquisition and analysis

For quantification of $Iba1^+$ cell density, images were acquired with a Leica DM6000 epifluorescence microscope equipped with a CCD camera (CoolSNAP EZ, Teledyne Photometrics). Density of $Iba1^+$ cells was quantified on 20x images collected in several regions (identified anatomically), including CA1, CA3 and dentate gyrus (DG) of the dorsal hippocampus, retrosplenial cortex (Ctx) and dLGN. For each region, one image per hemisphere was taken from four to six separate brain sections to obtain an average value for that mouse. Images were smooth processed and binarized, and $Iba1^+$ cells were identified and counted using the Analyze particle plugin for ImageJ, setting the minimum detectable size at 40 $µm^2$.

For 3D reconstruction of entire microglial cells and analysis of microglial lysosome content, confocal fluorescent images were acquired on an upright confocal microscope (Leica TCS SP5), using a 40x/1.25-0.75 oil (11506253) objective with 2X electronic magnification (188.92 nm pixel size) and lasers set at 488 and 561 nm for excitation of FITC and Cy3, respectively. Stacks were acquired using a 0.5 µm z-interval. Image stacks were imported into ImageJ for processing as previously described [62, 63]. Briefly, to edit the channel window containing $Iba1^+$ cells, an Unsharp Mask filter was used to further increase contrast using a pixel radius of 3 and mask weight of 0.6, a despeckle step was performed to remove salt-and-pepper noise and outlier pixels were removed with the Remove Outliers function (pixel radius 2; threshold 50). Image stacks were then imported into Imaris Software (Bitplane). Individual microglia were reconstructed in 3D using the filament tracer module and measures of the process length, terminal points, as well as 3D-Sholl analysis were performed to assess their morphology. For analysis of $CD68^+$ intracellular compartment, surface module was used to reconstruct the volume of individual Iba1+ cells and of CD68-labeled lysosomes, and then the percent of microglia volume occupied by CD68 was assessed as previously described [62]. The experimenter carrying out the acquisition and analysis of images was blind to the mice genotype.

DiI labeling of dendritic spines and analysis of microglial proximity

Deeply sedated mice (pentobarbital, 140 $mg.kg^{-1}$ i.p.) were transcardially perfused with 2% formaldehyde in PBS. Whole brains were removed, immersed in the same fixative for 1 h, transferred to a solution consisting of PBS with 0.01% sodium azide until being cut, and sectioned at 100 µm thickness on a vibratome (Leica). Two sections per mouse were selected in the region corresponding to 1.82 mm caudal to bregma in the mouse brain atlas of Franklin and Paxinos [61]. DiI labeling of dendritic spine and spine analysis were performed as previously described [64]. Briefly, DiI beads (1,10-dioctadecyl-3,3,30,30-tetramethylindocarbocyanine perchlorate; Molecular Probes, Eugene, OR) were delivered to the slices using a helium gas pressure (100–150 psi) through the gene gun device (BioRad). A 3 µm pore size filter (Isopore polycarbonate, Millipore) was inserted between the gene gun and the slice to select single beads. Slices were kept in PBS at room temperature for at least 2 h to allow DiI diffusion in neurons, then incubated in permeabilizing solution (0.1% triton in phosphate buffer, PB) for 5 min, followed by blocking solution (0.25% gelatin and 0.01% triton in PB) for 45 min. Rat anti-P2Y12 receptor (0.5 $µg.µL^{-1}$, Biolegend 848002) was diluted in a solution of 0.125% gelatin and 0.01% triton in PB and samples were incubated for 72 h at 4°C with gentle agitation. After rinsing three times with 0.125% gelatin and 0.01% triton in PB, donkey anti-rat 488 (0.0013 $µg.µL^{-1}$, Invitrogen A21208) was added to the buffer for 3h at room temperature. Slices were mounted in Mowiol containing DAPI (0.005 $µg.µL^{-1}$, Sigma). Image stacks of apical dendritic segments in CA1 were taken using a confocal laser scanning microscope (SP5, Leica) equipped with a 63x/1.4 NA objective (oil immersion, Leica) with a pinhole aperture set to 1 Airy unit, pixel size of 60 nm and z-step of 200 nm. The excitation wavelength and emission range were 488 and 500-550 nm for Alexa 488 (i.e., P2Y12 receptor) and 561 and 570-620 for DiI. Deconvolution with experimental point spread function from fluorescent beads using a maximum likelihood estimation algorithm was performed with Huygens software (Scientific Volume Imaging). One hundred fifty iterations were applied in classical mode, background intensity was averaged from the voxels with lowest intensity, and signal to noise ratio values were set to a value of 20. For each mouse, 10 dendritic segments of 20–50 µm in length were analyzed. Dendritic spines were analyzed with Neuronstudio software [65] (version 9.92; http://research.mssm.edu/cnic/tools.html). Images from the P2Y12 receptor channel were preprocessed in order to enhance the contrast, using an Unsharp Mask filter using a pixel

radius of 3 and mask weight of 0.6, a despeckle step was performed to remove salt-and-pepper noise and outlier pixels were removed with the Remove Outliers function (pixel radius 2; threshold 50). To analyze the interaction between microglial processes and dendritic spines, we measured the percentage of dendritic spines having microglial processes located within 0.3 µm surrounding the spine head using Fiji-ImageJ software. To assess the presence of microglial processes, for each spine, its 3D coordinates and head diameter measured with Neuronstudio were used to draw a sphere on the image using the DrawShape function of the plugin 3DImageSuite. A second sphere centered on the spine coordinates with a diameter extended by 0.3 µm was then drawn. The volume space in between the two spheres was converted into a Region of Interest. The mean intensity inside the 3D ring volume was assessed in the channel corresponding to Alexa 488 (i.e., P2Y12 receptor), and compared to that of the background. If the mean intensity was more than ten times than that of the background, it was considered that the spine had microglial processes in proximity.

Golgi staining and spine analysis

Fresh brains were processed following the Golgi-Cox method as described before [66, 67]. Briefly, mice were deeply sedated (pentobarbital, 140 $mg.kg^{-1}$ i.p.) and brains were harvested, briefly rinsed in NaCl, and incubated in the dark in filtered dye solution (10 $g.L^{-1}$ $K_2Cr_2O_7$, 10 $g.L^{-1}$ $HgCl_2$ and 8 $g.L^{-1}$ K_2CrO_4) for 15-16 days. Impregnated brains were then washed 3 × 2 min in distilled water (dH_2O) and transferred to a tissue-protectant solution (30% sucrose in dH_2O) for 24 h. Afterwards, brains were rinsed 3 x 2 min in dH_2O and incubated 30 min in 90% EtOH (v/v). Two hundred µm-thick coronal sections were cut in 70% EtOH on a vibratome (Leica) and washed in dH_2O for 5 min. Next, sections containing the dorsal hippocampus (6 sections per mouse), or medial prefrontal cortex (6 sections per mouse) were reduced in 16% ammonia solution for 1 h, washed in dH_2O for 2 min and fixated in 10 $g.L^{-1}$ $Na_2S_2O_3$ for 7 min. After a final wash in dH_2O, sections were mounted on superfrost slides and allowed to dry at room temperature for 1-2 h. The dehydration steps proceeded as following: 3 min in 50% EtOH, 3 min in 70% EtOH, 3 min in 80% EtOH and 3 min in 100% EtOH, 2 × 5 min in a 2:1 isopropanol:EtOH mixture, 5 min in pure isopropanol and 2 × 5 min in xylol. Neurons were first identified with a light microscope (Leica 6000) under low magnification (×20). At least three neurons per mouse were selected according to the following criteria: (1) consistent and dark impregnation along the entire extent of all the dendrites; (2) presence of fourth-order branches for both apical and basal dendrites, (3) presence of untruncated dendrites, (4) soma entirely within the thickness of the section, and (5) relative isolation from neighboring impregnated neurons. Bright-field images of z-stacks of apical dendrites from hippocampal CA1 and L2/L3 pyramidal neurons were then captured with a × 100 oil objective every 0.2 µm using a CoolSNAP EZ CCD Camera (Teledyne Photometrics). Given that protrusions density reached a plateau 45 µm away from the soma, we selected dendritic segments at least 50 µm away from the cell body. Protrusions were counted on secondary branches of apical dendrites. Only protrusions with a clear connection of the head of the protrusion to the shaft of the dendrite were counted. Protrusion density, length and width were analyzed using the Reconstruct software as described by Risher and colleagues [31]. Protrusions were classified based on their morphology into six classes using the following exclusive criteria [31]: filopodia, when the length value >2 µm; long thin spines, when the length value >1 µm and ≤2 µm; thin spines, when the length-to-width ratio (LWR) value >1; mushroom spines, when the width value >0.6 µm; stubby spines, when the LWR value ≤1; branched spines, when spines showed more than one head (entered manually by the experimenter). All image analyses were done blind.

Patch clamp recordings

Two hundred fifty µm-thick transverse hippocampal slices were prepared from brains of P15 mice. Mice were deeply sedated (pentobarbital, 140 $mg.kg^{-1}$ i.p.) and the brain was quickly removed from the skull, then sectioned with a vibroslicer (HM 650 V, Microm) in ice-cold artificial cerebrospinal fluid (ACSF) containing the following (in $mmol.L^{-1}$): 125 NaCl, 2.5 KCl, 25 glucose, 25 $NaHCO_3$, 1.25 NaH2PO_4, 2 $CaCl_2$, and 1 $MgCl_2$, continuously bubbled with 95% O2-5% CO_2. Slices were incubated in ACSF at 32°C for 20 min and then at room temperature (20-25°C). For patch-clamp recordings, slices were transferred to the recording chamber where they were continuously superfused with ACSF (30-32°C) buffered by continuous bubbling with 95% O_2-5% CO_2. Patch-clamp pipettes (4–6 Mohm resistance) were prepared from borosilicate glass (BF150-86-10; Harvard Apparatus) using a DMZ pipette puller (Zeitz). CA1 pyramidal neurons were visually identified using an upright microscope (Olympus BX51WI). Neurons were voltage-clamped using an EPC10 amplifier (HEKA Elektronik) and the following intracellular solution (in $mmol.L^{-1}$): 120 Cs-methane sulfonate, 10 CsCl, 10 Hepes, 10 Phosphocreatine, 0.2 EGTA, 8 NaCl, 2 ATP-Na_2, 3 QX 314 (pH 7.25, adjusted with CsOH). Miniature excitatory postsynaptic currents (mEPSCs) were recorded in CA1 pyramidal neurons at a holding potential of -65 mV in the presence of Tetrodotoxin (TTX, 0.5 µM, Hello Bio) and SR95531 hydrobromide (Gabazine, 10 µM, Hello Bio). At least 200 s of recording were analyzed for each cell. Series resistance was left uncompensated. Input resistance was monitored by voltage steps of −10 mV before and after mEPSC recordings. Experiments were discarded if the series resistance changed by more than 20% during the recording. Data acquisition was performed using Patchmaster software (Heka Elektronik). The junction potential (-14.9 mV) was uncorrected. Signals were low pass-filtered at 4 kHz before sampling at 20 kHz. Recordings were filtered offline at 2 kHz using Clampfit (Molecular Devices) and analyzed using MiniAnalysis (Synaptosoft). During patch-clamp recordings and analysis, the investigator was blind to the mouse genotype.

Anterograde labeling of retinogeniculate projections

P15-16 mice were anesthetized with ketamine–xylazine (100 and 10 $mg.kg^{-1}$, respectively, in 0.9% saline). Eyes were intravitreally injected using a glass micropipette with 1–5 µl of 0.2% cholera toxin subunit B (CTB) conjugated to Alexa Fluor 488 or 555 (Invitrogen) diluted in 1% DMSO. After 48 h, mice were deeply sedated (pentobarbital, 140 $mg.kg^{-1}$ i.p.) and perfused transcardially with 4% paraformaldehyde in PBS. Brains were postfixed overnight with the same fixative and sectioned with a vibratome (60 µm). All sections containing the dorsal lateral geniculate nucleus of the thalamus (dLGN) were selected and directly mounted in Mowiol containing DAPI (0.005 $µg.µL^{-1}$, Sigma). 10X epifluorescent images were obtained using a CCD camera (CoolSNAP EZ, Teledyne Photometrics) attached to an upright Leica 6000 microscope.

MetaMorph software (Molecular Devices) was used for quantitative analyses. All image analyses were done blindly to the mice genotypes. Quantification of eye-specific segregation was performed on images of Alexa Fluor 488-labeled contralateral/Alexa Fluor 555-labeled ipsilateral projections, as previously described by Rebsam and colleagues [68]. Briefly, variable thresholds were used for the contralateral projection and a fixed threshold for the ipsilateral projection. After outlining the boundary of the dLGN, we measured the pixel overlap between ipsilateral and contralateral projections at every 10th threshold value for the contralateral image. The proportion of dLGN occupied by ipsilateral axons was measured as a ratio of ipsilateral pixels to the total number of pixels in the dLGN region. Additionally, we quantified the areas occupied by ipsilateral and contralateral retinogeniculate projections and the extent of ipsilateral retinogeniculate

projections along the outer-inner axis (O-I axis), perpendicular to the surface of the dLGN, and the dorsomedial-ventrolateral axis (DM-VL axis), parallel to the surface of the dLGN, as previously described by Hayakawa and Kawasaki [69]. The extent of the ipsilateral projection along the O-I and DM-VM axes was measured by tracing a line between the two points delineating the maximal extent of the ipsilateral signal along the chosen axis. The extent of the ipsilateral projection along the dLGN axis is calculated by dividing the length of the ipsilateral projection by the dLGN length and is expressed as a percentage of dLGN length. For quantifying the areas occupied by ipsilateral retinogeniculate projections, thresholds (Ti) were determined as follows: Ti = Mi x 0.165, where Mi was the maximum signal intensity in five consecutive sections, the third of which was the section containing the largest dLGN area. The size of the area whose signal intensities were more than Ti was used as the size of ipsilateral retinogeniculate projections. For quantifying the areas occupied by contralateral retinogeniculate projections, thresholds (Tc) were determined as follows: Tc = Mc x 0.5, where Mc was the average signal intensity of contralateral retinogeniculate projections. The areas whose signal intensities were less than Tc consisted of two kinds of regions: the "gap," which is the CTB-negative area in the central dLGN, and the regions that are connected with the contours of the dLGN. In order to measure the size of the gap, the latter was excluded.

Behavioral assessment

Experiments were carried out in the light phase of the light/dark cycle (between 8:00 a.m. and 8:00 p.m.). For each behavioral test, mice were acclimatized to the testing room for at least 1 hr. Equipment was carefully swabbed with 35% ethanol between each mouse to eliminate odors. Behavioral tests were video recorded in real-time and analyzed off-line by an experimenter blinded to the experimental groups using the free event recorder JWatcher software (Blumstein & Daniel http://www.jwatcher.ucla.edu/).

Novelty-induced locomotion

Adult mice were individually placed in a cage with the same size of the home-cage containing a thin layer of fresh bedding and allowed to freely explore for 15 min. Total distance moved and mean velocity were scored during 3 5-min blocks.

Novelty-induced self-grooming

Adult mice were individually placed in a Plexiglas cylindrical arena (20 cm in diameter), and the total time spent performing face, body and/or tail grooming was scored for 5 min as previously described [70].

Homing test

P25 mice were subjected to a maternal homing test as previously described [71]. This test exploits the tendency of mice to maintain body contact with the mother and their siblings and tests olfactory, visual and motor capacities. Mice were separated from the mother for at least 30 min before testing. During habituation, individual juveniles were transferred to a Plexiglas arena (23 × 23 cm, walls 13 cm high) containing fresh bedding with a small amount of soiled nest (not including fecal boli) sprinkled into the opposite corner and allowed to explore for 5 min. Time spent in the starting, nest and neutral corners was measured. Subsequently, the mice were briefly removed to a holding cage while two wire-mesh tubes were placed into the neutral corners, one empty and one containing the animal's mother. Time spent in the four corners was scored.

Social interaction

Each experimental mouse was individually transferred to a novel cage. After 15 min of habituation, an unfamiliar juvenile mouse (7 weeks old) of the same sex and strain, used as a social stimulus, was introduced in the cage for 10 min. The following behavioral patterns were used to define social investigation: anogenital sniff (sniffing the anogenital area of the partner); nose sniff (sniffing the head and the snout region of the partner); body sniff (sniffing any other area of the body of the partner); allogrooming (grooming the partner). The duration of social investigation was measured.

Social flexibility

Social and aggressive behavior in response to a challenge in social hierarchy was recorded according to the paradigm previously described [72, 73]. Briefly, mice housed two by two of the same genotype were observed in their home cage, for a single 30 min session on two consecutive days. The cages had not been cleaned for seven days at the time of the observations, to allow impregnation of the bedding with animal's odors. During the first day of observation, no manipulation was performed. On the second day, the cage bedding was changed with clean bedding just before the session of observation. This procedure is known to challenge social hierarchy and to elicit aggressive behavior. The behavioral elements scored for duration were related to social investigation (sniffing and grooming the partner in all body regions indicative of affiliative behavior) or aggressive behavior (active fighting episode of attacks and aggressive grooming, as well as tail rattling and digging behaviors aimed to assess dominant status). Since the data collected was dependent, only one mouse, randomly selected from each cage, has been considered in the analysis. In order to be able to discriminate the two animals during data collection, one of the two experimental subjects was marked with a blue, scentless and nontoxic felt pen seven days before the first day of observation.

Reversal learning

To evaluate memory formation and cognitive flexibility, mice were subjected to a Y-maze task. The apparatus consisted of a transparent, Plexiglas maze composed of 3 test arms forming a Y. The entire procedure took 10 consecutive days: 1 day of habituation, 6 days of acquisition and 3 days of reversal learning. One of the arms was randomly selected as starting arm and, during habituation, mice were individually located in the maze, free to explore for 30 min. In the acquisition phase, one of the other two was baited with a food reward pellet (Noyes sucrose pellet, 20 mg, Research Diets, Inc., New Brunswick, NJ). The side of the rewarded arm was balanced across mice in order to avoid any side preference. Mice were trained to find the food reward in 10 consecutive trials for 6 days. If the mouse made the correct choice, it was given time to consume the sugar pellet, and then guided back into the start arm for the next trial. Incorrect choices were not rewarded or punished. If the mouse did not make any choice in 3 min, it went back to the home cage and the trial was considered as incorrect. For each successive trial, the reward was always placed in the same arm. Number of errors in arm selection, and number of days to criterion were recorded by an observer, blind to the genotypes. The % of correct choice of one session (i.e., day) is the ratio of the number of correct choices divided by the number of trials (=10). The criterion for task acquisition, determined for each mouse, was 80% correct responses on three consecutive days. Each mouse that met criterion for acquisition was then further assessed using a reversal procedure, in which the reward location was switched to the arm opposite to its previous location for each mouse. Ten trials per day were then performed for reversal learning, using the same methods and criterion as described above. Subjects were food-restricted, maintaining them at 80-85% of their

individual body weight calculated under ad libitum feeding conditions, starting 1 week before the beginning of the experiment and throughout the entire procedure.

Olfactory habituation/dishabituation test

The ability to discriminate non-social and social odors was measured using modifications of the olfactory habituation/dishabituation task, as previously described [74]. Subjects were individually tested for time spent sniffing cotton tipped swabs suspended from the cage lid. The olfactory cues were designed to measure familiar and unfamiliar odors, with and without social valence. Sequences of three identical swabs assayed habituation to the same odor, resulting in a progressive decrease in olfactory investigation. Switching to a different odor on the swab assayed dishabituation, i.e., recognition that an odor is new. Five different odors were presented in three consecutive trials of 2 min per trial, with an inter-trial interval of 1 min. The order of swaps was water (neutral odor), two non-social odors (almond and banana) and two social scents (social 1, unfamiliar mouse of the same sex and different strain, and social 2, unfamiliar mouse of the same strain and opposite sex). In each session trials 50 μL H_2O or 50 μL of a 1:100 dilution of the odor solutions in H_2O were pipetted onto a new cotton applicator directly before the test and sealed in a closed tube until the presentation. Unfamiliar social scents were prepared on the test day by swapping the bottom of a cage with a mouse from a different strain (i.e., C57BL/6J) or opposite sex on a cotton applicator and kept sealed until the presentation. Time spent sniffing the swab was quantitated with a stopwatch by a blinded human observer. Sniffing was scored when the nose was within 2 cm of the cotton swab. Each test session was conducted in a clean mouse cage containing fresh litter.

Statistical analysis

For each figure, the *n* values are summarized at the end of the legend. Statistical analyses were performed using GraphPad Prism 6.01 software (Graph-Pad Software). Males and females were included and compared to determine if sex impacted our experimental results. All *n* values represent individual animals, unless stated otherwise (i.e., electrophysiology experiments). Notably, in analyses where multiple microglia were assayed per animal, all microglia analyzed for an individual animal were averaged to generate a single value per animal. When appropriate, animals were randomly assigned to conditions. Where possible, conditions were randomized to account for potential ordering effects. To ensure reproducibility, when relevant, experiments were performed at least three times independently. To avoid litter bias in the mouse experiments, experimental groups were composed of animals from different litters randomly distributed. All analyses were conducted with blinding to the experimental condition. Data are presented as scatter dot plot with bar, and the line at the mean ± S.E.M. (standard error of the mean). Comparisons between two groups following a normal distribution were analyzed using two-tailed unpaired t-test with or without Welch's correction, comparisons between two groups not following a normal distribution with Mann-Whitney test. Normality was assessed using the D'Agostino & Pearson omnibus normality test. When we compared cumulative distributions, we used the Kolmogorov-Smirnov test. When more than one variable was evaluated, we employed the two-way ANOVA with or without repeated measures (ANOVA and RM-ANOVA, respectively) with Sidak multiplicity-corrected post hoc comparisons to compare cohorts where appropriate. We didn't exclude samples for analysis (in some instances experimental data were tested for the presence of outliers using the Grubbs' test and alpha = 0,05 https://www.graphpad.com/quickcalcs/grubbs1/, but we didn't identify outliers). The statistical tests are reported in the figure legends along with the definition of *n*. For all analyses, $\alpha = 0.05$.

Acknowledgements

We thank Chris N. Parkhurst and Wenbiao B. Gan for providing the *Cx3cr1*^{creERT2} knock-in mice, the *Cell* and *Tissue Imaging Facility* of the Institut du Fer à Moulin (namely Theano Eirinopoulou, Mythili Savariradjane and Xavier Marquès), where all image acquisitions and analyses have been performed, and the staff of the IFM animal facility (namely Baptiste Lecomte, Gaël Grannec, François Baudon, Anna-Sophia Mourenco, Emma Courteau and Eloise Marsan). We warmly thank Patricia Gaspar, Ludmilla Lokmane, Sonia Garel, Véronique Fabre and Jean Christophe Poncer for the discussion and revision. This work has been supported by grants from the Agence Nationale de la Recherche (ANR-17-CE16-0008, ANR-11-IDEX-0004-02), the Fondation pour la Recherche Médicale (Equipe FRM DEQ2014039529) and the Fédération pour la Recherche sur le Cerveau (FRC-2019-19F10).

Author contributions

G.A., I.D., L.M. and A.Ro. designed the studies. G.A., I.D, A. Ro and L.M. wrote the manuscript, all authors revised it. G.A., I.D., F.E. and C.B. performed tamoxifen administration. G.A. performed immunofluorescence, image acquisition and analysis, Golgi-Cox staining and spine analyses. N.H. contributed to the design of DiOlistic labeling of dendritic spines, provided reagents and created the ImageJ Macro to analyze microglia/spines proximity. G.A. delivered DiI, performed image acquisition and analysis. C.L.M. contributed to the design and analysis of the electrophysiology experiments and provided reagents. G.A., M.D. and N.R.N. performed the electrophysiology experiments. A.Re. contributed to the design and analysis of the anterograde labeling of retinogeniculate projections and G.A. performed the intravitreal injections and image acquisition and analysis. I.D. performed behavioral experiments. G.A., I.D. and M.D. performed data analysis.

Competing interests

The authors declare no competing interests.

References

1. Thion MS, Ginhoux F, Garel S. Microglia and early brain development: An intimate journey. Science. 2018;362:185–189.
2. Conio B, Martino M, Magioncalda P, Escelsior A, Inglese M, Amore M, et al. Opposite effects of dopamine and serotonin on resting-state networks: review and implications for psychiatric disorders. Mol Psychiatry. 2020;25:82–93.
3. Lin S-H, Lee L-T, Yang YK. Serotonin and Mental Disorders: A Concise Review on Molecular Neuroimaging Evidence. Clin Psychopharmacol Neurosci. 2014;12:196–202.
4. Marazziti D. Understanding the role of serotonin in psychiatric diseases. F1000Res. 2017;6:180.
5. Anderson GM, Horne WC, Chatterjee D, Cohen DJ. The Hyperserotonemia of Autism. Ann NY Acad Sci. 1990;600:331–340.
6. Gabriele S, Sacco R, Persico AM. Blood serotonin levels in autism spectrum disorder: a systematic review and meta-analysis. Eur Neuropsychopharmacol. 2014;24:919–929.

7. Migliarini S, Pacini G, Pelosi B, Lunardi G, Pasqualetti M. Lack of brain serotonin affects postnatal development and serotonergic neuronal circuitry formation. Mol Psychiatry. 2013;18:1106–1118.
8. Witteveen JS, Middelman A, van Hulten JA, Martens GJM, Homberg JR, Kolk SM. Lack of serotonin reuptake during brain development alters rostral raphe-prefrontal network formation. Front Cell Neurosci. 2013;7.
9. Teissier A, Soiza-Reilly M, Gaspar P. Refining the Role of 5-HT in Postnatal Development of Brain Circuits. Front Cell Neurosci. 2017;11:139.
10. Kolodziejczak M, Béchade C, Gervasi N, Irinopoulou T, Banas SM, Cordier C, et al. Serotonin Modulates Developmental Microglia via 5-HT $_{2B}$ Receptors: Potential Implication during Synaptic Refinement of Retinogeniculate Projections. ACS Chem Neurosci. 2015;6:1219–1230.
11. Krabbe G, Matyash V, Pannasch U, Mamer L, Boddeke HWGM, Kettenmann H. Activation of serotonin receptors promotes microglial injury-induced motility but attenuates phagocytic activity. Brain, Behavior, and Immunity. 2012;26:419–428.
12. Béchade C, D'Andrea I, Etienne F, Verdonk F, Moutkine I, Banas SM, et al. The serotonin 2B receptor is required in neonatal microglia to limit neuroinflammation and sickness behavior in adulthood. Glia. 2021;69:638–654.
13. Etienne F, Mastrolia V, Maroteaux L, Girault J-A, Gervasi N, Roumier A. Two-photon Imaging of Microglial Processes' Attraction Toward ATP or Serotonin in Acute Brain Slices. JoVE. 2019:58788.
14. Schafer DP, Lehrman EK, Kautzman AG, Koyama R, Mardinly AR, Yamasaki R, et al. Microglia Sculpt Postnatal Neural Circuits in an Activity and Complement-Dependent Manner. Neuron. 2012;74:691–705.
15. Upton AL, Salichon N, Lebrand C, Ravary A, Blakely R, Seif I, et al. Excess of Serotonin (5-HT) Alters the Segregation of Ispilateral and Contralateral Retinal Projections in Monoamine Oxidase A Knock-Out Mice: Possible Role of 5-HT Uptake in Retinal Ganglion Cells During Development. J Neurosci. 1999;19:7007–7024.
16. Gaspar P, Cases O, Maroteaux L. The developmental role of serotonin: news from mouse molecular genetics. Nat Rev Neurosci. 2003;4:1002–1012.
17. Pitychoutis PM, Belmer A, Moutkine I, Adrien J, Maroteaux L. Mice Lacking the Serotonin Htr2B Receptor Gene Present an Antipsychotic-Sensitive Schizophrenic-Like Phenotype. Neuropsychopharmacol. 2015;40:2764–2773.
18. Diaz SL, Doly S, Narboux-Nême N, Fernández S, Mazot P, Banas SM, et al. 5-HT2B receptors are required for serotonin-selective antidepressant actions. Mol Psychiatry. 2012;17:154–163.
19. Doly S, Quentin E, Eddine R, Tolu S, Fernandez SP, Bertran-Gonzalez J, et al. Serotonin 2B Receptors in Mesoaccumbens Dopamine Pathway Regulate Cocaine Responses. J Neurosci. 2017;37:10372–10388.
20. Nikodemova M, Kimyon RS, De I, Small AL, Collier LS, Watters JJ. Microglial numbers attain adult levels after undergoing a rapid decrease in cell number in the third postnatal week. Journal of Neuroimmunology. 2015;278:280–288.
21. Dalmau I, Vela JM, González B, Finsen B, Castellano B. Dynamics of microglia in the developing rat brain: Proliferation and Death of Microglia in Immature Brain. J Comp Neurol. 2003;458:144–157.

22. Weinhard L, di Bartolomei G, Bolasco G, Machado P, Schieber NL, Neniskyte U, et al. Microglia remodel synapses by presynaptic trogocytosis and spine head filopodia induction. Nat Commun. 2018;9:1228.
23. Vainchtein ID, Chin G, Cho FS, Kelley KW, Miller JG, Chien EC, et al. Astrocyte-derived interleukin-33 promotes microglial synapse engulfment and neural circuit development. Science. 2018;359:1269–1273.
24. Stevens B, Allen NJ, Vazquez LE, Howell GR, Christopherson KS, Nouri N, et al. The Classical Complement Cascade Mediates CNS Synapse Elimination. Cell. 2007;131:1164–1178.
25. Basilico B, Pagani F, Grimaldi A, Cortese B, Di Angelantonio S, Weinhard L, et al. Microglia shape presynaptic properties at developing glutamatergic synapses. Glia. 2019;67:53–67.
26. Filipello F, Morini R, Corradini I, Zerbi V, Canzi A, Michalski B, et al. The Microglial Innate Immune Receptor TREM2 Is Required for Synapse Elimination and Normal Brain Connectivity. Immunity. 2018;48:979-991.e8.
27. Paolicelli RC, Bolasco G, Pagani F, Maggi L, Scianni M, Panzanelli P, et al. Synaptic Pruning by Microglia Is Necessary for Normal Brain Development. Science. 2011;333:1456–1458.
28. Weinhard L, Neniskyte U, Vadisiute A, di Bartolomei G, Aygün N, Riviere L, et al. Sexual dimorphism of microglia and synapses during mouse postnatal development: Sexual Dimorphism in Microglia and Synapses. Devel Neurobio. 2018;78:618–626.
29. Cheadle L, Rivera SA, Phelps JS, Ennis KA, Stevens B, Burkly LC, et al. Sensory Experience Engages Microglia to Shape Neural Connectivity through a Non-Phagocytic Mechanism. Neuron. 2020;108:451-468.e9.
30. Miyamoto A, Wake H, Ishikawa AW, Eto K, Shibata K, Murakoshi H, et al. Microglia contact induces synapse formation in developing somatosensory cortex. Nat Commun. 2016;7:12540.
31. Risher WC, Ustunkaya T, Singh Alvarado J, Eroglu C. Rapid Golgi Analysis Method for Efficient and Unbiased Classification of Dendritic Spines. PLoS ONE. 2014;9:e107591.
32. Assali A, Gaspar P, Rebsam A. Activity dependent mechanisms of visual map formation--from retinal waves to molecular regulators. Semin Cell Dev Biol. 2014;35:136–146.
33. Brioschi S, d'Errico P, Amann LS, Janova H, Wojcik SM, Meyer-Luehmann M, et al. Detection of Synaptic Proteins in Microglia by Flow Cytometry. Front Mol Neurosci. 2020;13:149.
34. D'Andrea I, Alleva E, Branchi I. Communal nesting, an early social enrichment, affects social competences but not learning and memory abilities at adulthood. Behavioural Brain Research. 2007;183:60–66.
35. May T, Adesina I, McGillivray J, Rinehart NJ. Sex differences in neurodevelopmental disorders. Current Opinion in Neurology. 2019;32:622–626.
36. van den Berg WE, Lamballais S, Kushner SA. Sex-Specific Mechanism of Social Hierarchy in Mice. Neuropsychopharmacol. 2015;40:1364–1372.
37. Zhan Y, Paolicelli RC, Sforazzini F, Weinhard L, Bolasco G, Pagani F, et al. Deficient neuron-microglia signaling results in impaired functional brain connectivity and social behavior. Nat Neurosci. 2014;17:400–406.
38. Parkhurst CN, Yang G, Ninan I, Savas JN, Yates JR, Lafaille JJ, et al. Microglia Promote Learning-Dependent Synapse Formation through Brain-Derived Neurotrophic Factor. Cell. 2013;155:1596–1609.

39. Badimon A, Strasburger HJ, Ayata P, Chen X, Nair A, Ikegami A, et al. Negative feedback control of neuronal activity by microglia. Nature. 2020;586:417–423.
40. Cserép C, Pósfai B, Lénárt N, Fekete R, László ZI, Lele Z, et al. Microglia monitor and protect neuronal function through specialized somatic purinergic junctions. Science. 2020;367:528–537.
41. Akiyoshi R, Wake H, Kato D, Horiuchi H, Ono R, Ikegami A, et al. Microglia Enhance Synapse Activity to Promote Local Network Synchronization. ENeuro. 2018;5:ENEURO.0088-18.2018.
42. Assali A, Le Magueresse C, Bennis M, Nicol X, Gaspar P, Rebsam A. RIM1/2 in retinal ganglion cells are required for the refinement of ipsilateral axons and eye-specific segregation. Sci Rep. 2017;7:3236.
43. Thion MS, Low D, Silvin A, Chen J, Grisel P, Schulte-Schrepping J, et al. Microbiome Influences Prenatal and Adult Microglia in a Sex-Specific Manner. Cell. 2018;172:500-516.e16.
44. Villa A. Sexual differentiation of microglia. Frontiers in Neuroendocrinology. 2019:9.
45. Hanamsagar R, Alter MD, Block CS, Sullivan H, Bolton JL, Bilbo SD. Generation of a microglial developmental index in mice and in humans reveals a sex difference in maturation and immune reactivity: HANAMSAGAR et al. Glia. 2017;65:1504–1520.
46. Jovanovic H, Lundberg J, Karlsson P, Cerin Å, Saijo T, Varrone A, et al. Sex differences in the serotonin 1A receptor and serotonin transporter binding in the human brain measured by PET. NeuroImage. 2008;39:1408–1419.
47. Ohsawa K, Irino Y, Sanagi T, Nakamura Y, Suzuki E, Inoue K, et al. P2Y $_{12}$ receptor-mediated integrin-β1 activation regulates microglial process extension induced by ATP. Glia. 2010. 2010. https://doi.org/10.1002/glia.20963.
48. Sipe GO, Lowery, RL, Tremblay M-È, Kelly EA, Lamantia CE, Majewska AK. Microglial P2Y12 is necessary for synaptic plasticity in mouse visual cortex. Nat Commun. 2016;7:10905.
49. Maroteaux L, Béchade C, Roumier A. Dimers of serotonin receptors: Impact on ligand affinity and signaling. Biochimie. 2019;161:23–33.
50. von Kügelgen I, Hoffmann K. Pharmacology and structure of P2Y receptors. Neuropharmacology. 2016;104:50–61.
51. Oliver KH, Duvernay MT, Hamm HE, Carneiro AMD. Loss of Serotonin Transporter Function Alters ADP-mediated Glycoprotein αIIbβ3 Activation through Dysregulation of the 5-HT2A Receptor. Journal of Biological Chemistry. 2016;291:20210–20219.
52. Baqi Y, Müller CE. Antithrombotic P2Y12 receptor antagonists: recent developments in drug discovery. Drug Discovery Today. 2019;24:325–333.
53. Saini HK, Takeda N, Goyal RK, Kumamoto H, Arneja AS, Dhalla NS. Therapeutic Potentials of Sarpogrelate in Cardiovascular Disease*. Cardiovascular Drug Reviews. 2006;22:27–54.
54. Percie du Sert N, Hurst V, Ahluwalia A, Alam S, Avey MT, Baker M, et al. The ARRIVE guidelines 2.0: Updated guidelines for reporting animal research. PLoS Biol. 2020;18:e3000410.
55. Belmer A, Quentin E, Diaz SL, Guiard BP, Fernandez SP, Doly S, et al. Positive regulation of raphe serotonin neurons by serotonin 2B receptors. Neuropsychopharmacol. 2018;43:1623–1632.
56. Pitulescu ME, Schmidt I, Benedito R, Adams RH. Inducible gene targeting in the neonatal vasculature and analysis of retinal angiogenesis in mice. Nat Protoc. 2010;5:1518–1534.

57. Goldmann T, Wieghofer P, Müller PF, Wolf Y, Varol D, Yona S, et al. A new type of microglia gene targeting shows TAK1 to be pivotal in CNS autoimmune inflammation. Nat Neurosci. 2013;16:1618–1626.
58. Peng J, Gu N, Zhou L, B Eyo U, Murugan M, Gan W-B, et al. Microglia and monocytes synergistically promote the transition from acute to chronic pain after nerve injury. Nat Commun. 2016;7:12029.
59. Wolf Y, Yona S, Kim K-W, Jung S. Microglia, seen from the CX3CR1 angle. Front Cell Neurosci. 2013;7.
60. Yona S, Kim K-W, Wolf Y, Mildner A, Varol D, Breker M, et al. Fate Mapping Reveals Origins and Dynamics of Monocytes and Tissue Macrophages under Homeostasis. Immunity. 2013;38:79–91.
61. Franklin KBJ, Paxinos G. Paxino's and Franklin's the Mouse Brain in Stereotaxic Coordinates: Compact 5th Edition. San Diego: Elsevier Science & Technology; 2019.
62. Schafer DP, Lehrman EK, Heller CT, Stevens B. An Engulfment Assay: A Protocol to Assess Interactions Between CNS Phagocytes and Neurons. JoVE. 2014:51482.
63. Young K, Morrison H. Quantifying Microglia Morphology from Photomicrographs of Immunohistochemistry Prepared Tissue Using ImageJ. JoVE. 2018:57648.
64. Heck N, Betuing S, Vanhoutte P, Caboche J. A deconvolution method to improve automated 3D-analysis of dendritic spines: application to a mouse model of Huntington's disease. Brain Struct Funct. 2012;217:421–434.
65. Rodriguez A, Ehlenberger DB, Dickstein DL, Hof PR, Wearne SL. Automated Three-Dimensional Detection and Shape Classification of Dendritic Spines from Fluorescence Microscopy Images. PLoS ONE. 2008;3:e1997.
66. Giralt A, Brito V, Chevy Q, Simonnet C, Otsu Y, Cifuentes-Díaz C, et al. Pyk2 modulates hippocampal excitatory synapses and contributes to cognitive deficits in a Huntington's disease model. Nat Commun. 2017;8:15592.
67. Zaqout S, Kaindl AM. Golgi-Cox Staining Step by Step. Front Neuroanat. 2016;10.
68. Rebsam A, Petros TJ, Mason CA. Switching Retinogeniculate Axon Laterality Leads to Normal Targeting but Abnormal Eye-Specific Segregation That Is Activity Dependent. Journal of Neuroscience. 2009;29:14855–14863.
69. Hayakawa I, Kawasaki H. Rearrangement of Retinogeniculate Projection Patterns after Eye-Specific Segregation in Mice. PLoS ONE. 2010;5:e11001.
70. Silverman JL, Tolu SS, Barkan CL, Crawley JN. Repetitive Self-Grooming Behavior in the BTBR Mouse Model of Autism is Blocked by the mGluR5 Antagonist MPEP. Neuropsychopharmacol. 2010;35:976–989.
71. Scattoni ML, Gandhy SU, Ricceri L, Crawley JN. Unusual Repertoire of Vocalizations in the BTBR T+tf/J Mouse Model of Autism. PLoS ONE. 2008;3:e3067.
72. D'Andrea I, Fardella V, Fardella S, Pallante F, Ghigo A, Iacobucci R, et al. Lack of kinase-independent activity of PI3Kγ in locus coeruleus induces ADHD symptoms through increased CREB signaling. EMBO Mol Med. 2015;7:904–917.
73. D'Andrea I, Alleva E, Branchi I. Communal nesting, an early social enrichment, affects social competences but not learning and memory abilities at adulthood. Behav Brain Res. 2007;183:60–66.
74. Yang M, Crawley JN. Simple Behavioral Assessment of Mouse Olfaction. Current Protocols in Neuroscience. 2009;48.

Table and Figures legends

Time of invalidation of *Htr2b* in microglia	**Age at the time of the analysis**	**Sex**	**Analyses performed**
"Early" invalidation (tamoxifen P1-P5), i.e., “birth” subscript	P15	Males and females	Immunohistochemistry to study microglia, DiI/P2Y12 receptor labeling, Golgi staining, patch clamp recordings
	P15-P18	Males and females	Anterograde labeling (P15) and analysis (P18) of retinogeniculate projections
	P25 (maternal homing test), P80-P120	Males and females	Behavioral assessment
"Late" invalidation (tamoxifen P28-P32), i.e., “P30” subscript	P80-P120	Males and females	Behavioral assessment

Table 1. Tamoxifen administration and experimental design

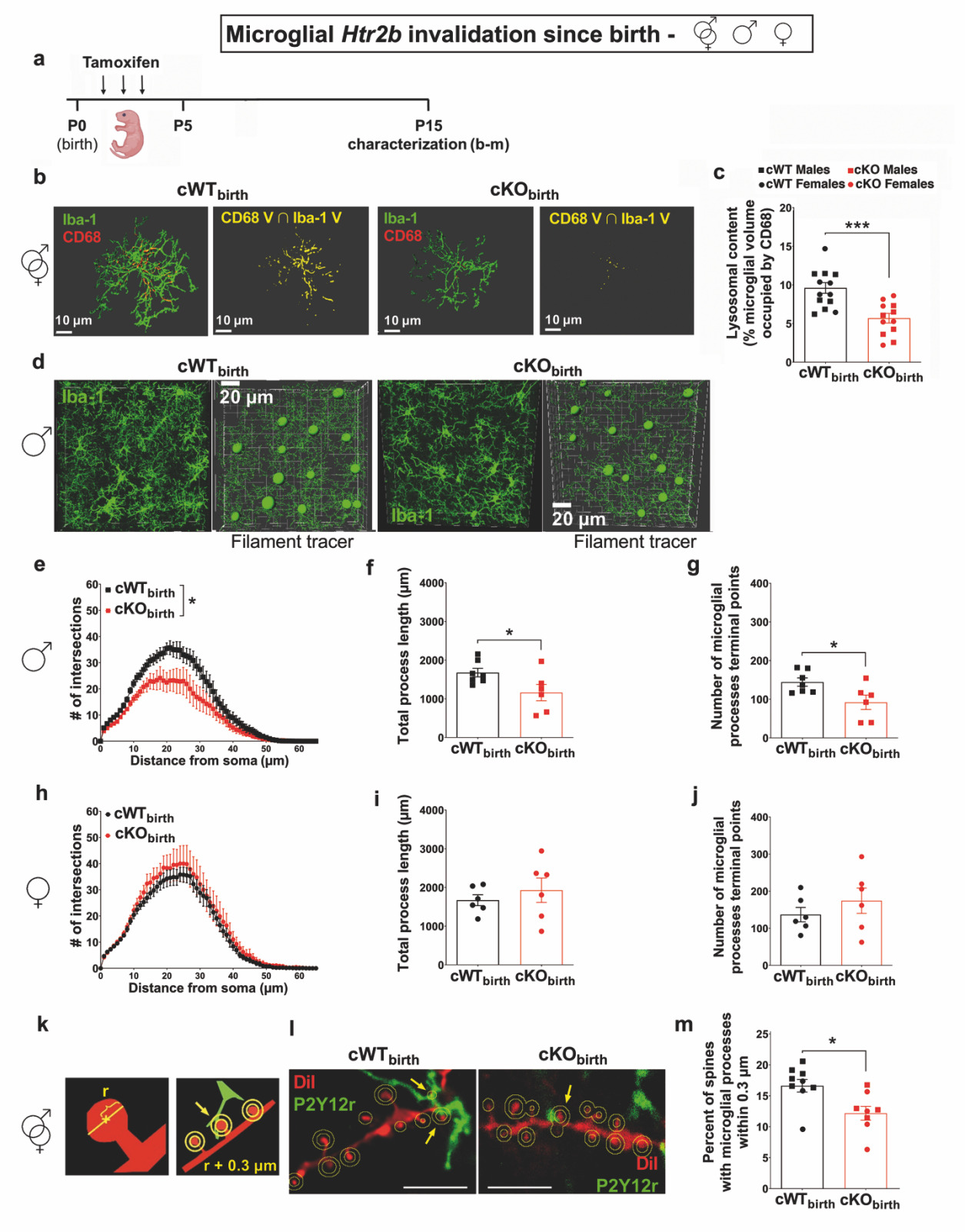

Fig. 1 | Absence of 5-HT$_{2B}$ receptors in neonatal microglia decreases their lysosome content, alters their morphology, and impacts the synapse-microglia proximity in the developing

hippocampus (CA1). a, Timeline of tamoxifen treatment for early *Htr2b* invalidation in microglia, and the analyses performed at P15. **b**, Representative images of CA1 microglia with their lysosomal content in cWT_{birth} and cKO_{birth} P15 mice. Left panels: immunostaining for Iba1 and the microglial lysosomal protein CD68; right panels: 3D reconstruction of $CD68^+$ lysosomes with $Iba1^+$ cells overlay (in yellow). **c,** The relative microglial cell volume occupied by $CD68^+$ lysosomes in CA1 is significantly reduced in cKO_{birth} mice (cWT_{birth}, n = 13 mice, mixed males and females; cKO_{birth}, n = 12 mice, mixed males and females; 8 microglia analyzed and averaged per animal; unpaired t-test with Welsh's correction, p = 0.0003). **(d-g)** Morphological analysis of CA1 microglia in P15 male mice (cWT_{birth}, n = 7 male mice; cKO_{birth}, n = 6 male mice; for each mouse, the value represents the average value of 4-8 microglia). **d**, Representative images of microglia ($Iba1^+$ cells, left panels) in CA1 of cWT_{birth} and cKO_{birth} P15 male mice, and their 3D reconstructions (right panels) carried out using the filament tracer module by Imaris. **e**, Sholl profiles; note the reduced arborization in microglia from cKO_{birth} males compared to cWT_{birth} (two-way RM-ANOVA: significant main effects of interaction $P < 0.0001$, $F_{65,715} = 2.571$, radius $P < 0.0001$, $F_{65,715} = 65.13$ and genotype $P = 0.0295$, $F_{1,11} = 6.254$). **f**, Total length of microglial processes; note the reduction in cKO_{birth} (Mann-Whitney test, p = 0.0350). **g**, Number of microglial processes terminal points; note the reduced number of terminal points in cKO_{birth} (Mann-Whitney test, p = 0.0408). **(h-j)** Morphological analysis of CA1 microglia in P15 female mice (cWT_{birth}, n = 6 female mice; cKO_{birth}, n = 6 female mice; for each mouse, the value represents the average value of 4-8 microglia). **h**, Similar Sholl profiles of microglia in cWT_{birth} and cKO_{birth} female mice. **i**, Similar total length of microglial processes in cWT_{birth} and cKO_{birth} female mice. **j**, Similar number of microglial processes terminal points in cWT_{birth} and cKO_{birth} female mice. **(k-m)**, Assessment of the association of dendritic spines with microglial processes at P15 in CA1. **k,** Drawings of the method used for quantification: a spine was counted as associated with a microglial process when microglial P2Y12 receptor (P2Y12r) staining was present at a distance < 0.3 µm. **l,** Representative images of hippocampal dendrites of cWT_{birth} and cKO_{birth} mice with some spines surrounded (arrows) by microglial processes ($P2Y12r^+$) in close proximity (< 0.3 µm). Analysis was performed in 3D in image stacks, the figure is represented in 2D for easier visualization. Scale bar: 5 µm. **m**, The percent of spines located within 0.3 µm to microglial processes was significantly reduced in cKO_{birth} mice (cWT_{birth} mice, n = 9 mice, mixed males and females; cKO_{birth} mice, n = 8 mice, mixed males and females; Mann-Whitney test, P = 0.0111). All graphs show mean±s.e.m. and points in (**c**, **f, g**, **i, j**, **and m**) represent individual animals. *p< 0.05, ***p < 0.005. Square symbols: males; round: females.

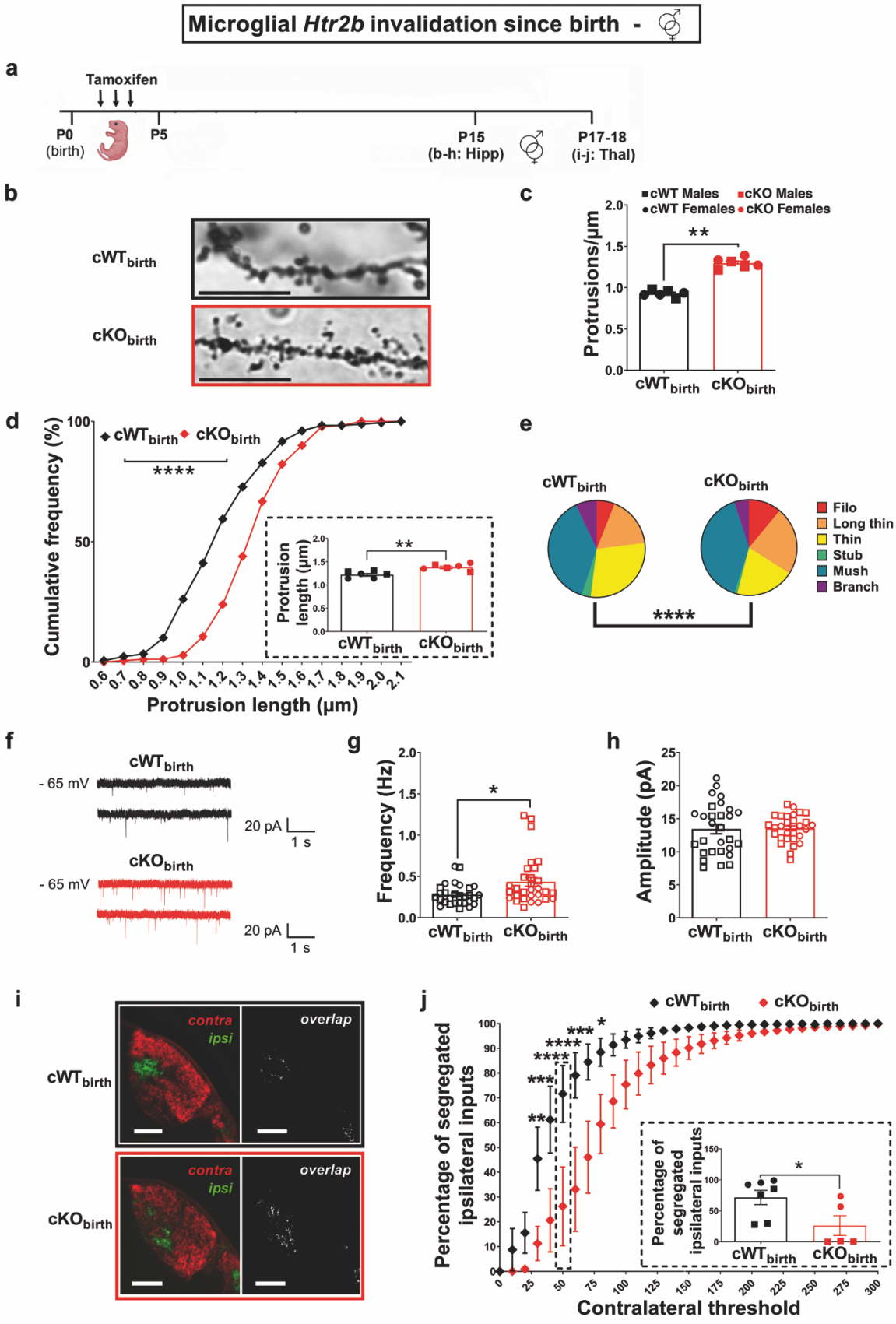
Microglial Htr2b invalidation since birth -
a
Tamoxifen
P0 (birth)
P5
P15 (b-h: Hipp)
P17-18 (i-j: Thal)
b
cWT birth
cKO birth
c
cWT Males
cKO Males
cWT Females
cKO Females
Protrusions/µm
**
d
cWT birth
cKO birth
****
Cumulative frequency (%)
Protrusion length (µm)
Protrusion length (µm)
**
e
cWT birth
cKO birth
Filo
Long thin
Thin
Stub
Mush
Branch
****
f
cWT birth
- 65 mV
20 pA
1 s
cKO birth
- 65 mV
20 pA
1 s
g
Frequency (Hz)
*
h
Amplitude (pA)
i
contra
ipsi
overlap
cWT birth
cKO birth
j
cWT birth
cKO birth
Percentage of segregated ipsilateral inputs
Contralateral threshold
Percentage of segregated ipsilateral inputs
*

Fig. 2 | Absence of 5-HT$_{2B}$ receptors in microglia since birth impairs neuronal circuits refinement in the developing hippocampus and thalamus. a, Timeline of tamoxifen treatment for early *Htr2b* invalidation in microglia, and analyses of hippocampal synapses at P15 or of dLGN axonal segregation at P17-18. Data on males and females are pooled. **(b-e)** Analysis of dendritic protrusions on CA1 pyramidal neurons in cWT$_{birth}$ and cKO$_{birth}$ mice at P15 (n = 6 mice/genotype, 30 dendrites per mouse). **b**, Representative images of secondary apical dendrites in hippocampal pyramidal neurons of cWT$_{birth}$ and cKO$_{birth}$ P15 mice labeled with Golgi staining, scale bar: 10 μm. **c**, Protrusions density on secondary apical dendrites; note the significant increase in cKO$_{birth}$ mice (Mann-Whitney test, p = 0.0022). **d**, Cumulative distribution plot for the average length of protrusions on secondary apical dendrites; note the significant rightward shift in cKO$_{birth}$ mice (n = 180 dendrites from 6 mice/genotype, Kolmogorov-Smirnov test, p < 0.0001). In the inset, quantification of protrusion length obtained averaging 30 dendrites/mouse, which confirms a significant increase in cKO$_{birth}$ mice (Mann-Whitney test, p = 0.0087). **e**, Pie charts showing the altered distribution of protrusion types in cKO$_{birth}$ mice (n = 180 dendrites from 6 mice/genotype, Chi-square test, p < 0.0001). Abbreviations: Filo: filopodia; Stub: stubby; Mush: mushroom. **(f-h)** Analysis of mEPSCs in CA1 in cWT$_{birth}$ (n = 29 cells from 5 mice) or cKO$_{birth}$ mice (n = 30 cells from 5 mice) at P15. **f**, Representative traces of mEPSC recordings in CA1 hippocampal acute slices from cWT$_{birth}$ and cKO$_{birth}$ mice. **g**, Increased mESPC frequency in cKO$_{birth}$ mice (Mann-Whitney test, p = 0.0120). **h**, Similar mESPC amplitude in cWT$_{birth}$ and cKO$_{birth}$ mice. **(i-j)** Analysis of dye-labeled retinogeniculate projections in dLGN of cWT$_{birth}$ and cKO$_{birth}$ mice (n = 7 and 5 mice, respectively) at P17-P18, 48h after intravitreal injection of AlexaFluor 488 or 555 in either eye. **i**, Representative images of axonal segregation in cWT$_{birth}$ and cKO$_{birth}$ mice. Left panels: projections from retinal ganglion cells from the ipsilateral retina are in green and those from the contralateral retina are in red; right panels: overlap between ipsi- and contralateral projections. Scale bars 100 μm. **j**, Percentage of pixels containing only ipsilateral signal (no contralateral signal) as a function of contralateral threshold (ipsilateral threshold is fixed); note the significant rightward shift in cKO$_{birth}$ mice, that demonstrate that ipsilateral fibers are less segregated from contralateral fibers (thus more overlapped) than in cWT$_{birth}$ mice (two-way RM-ANOVA: significant main effects of interaction P < 0.0001, $F_{30,300}$ = 4.118, contralateral threshold P = 0.0288, $F_{30,300}$ = 76.03 and genotype P = 0.0295, $F_{1,10}$ = 6.507; Sidak multiple comparisons: 30, p = 0.0027; 40, p = 0.0001; 50, p < 0.0001; 60, p < 0.0001; 70, p = 0.0003; 80, p = 0.0256. The inset shows a columnar representation of the values for the contralateral threshold set at 50 (Mann-Whitney test, p = 0.0303). All graphs (except cumulative curve in **d** and pie chart in **e**) show mean±s.e.m. and points in (**c**, inset of **d, g, h**, and inset of **j**) represent individual animals. *p < 0.05, **p < 0.01, ***p < 0.005, ****p < 0.0001. Square symbols: males; round: females; diamond: mixed.

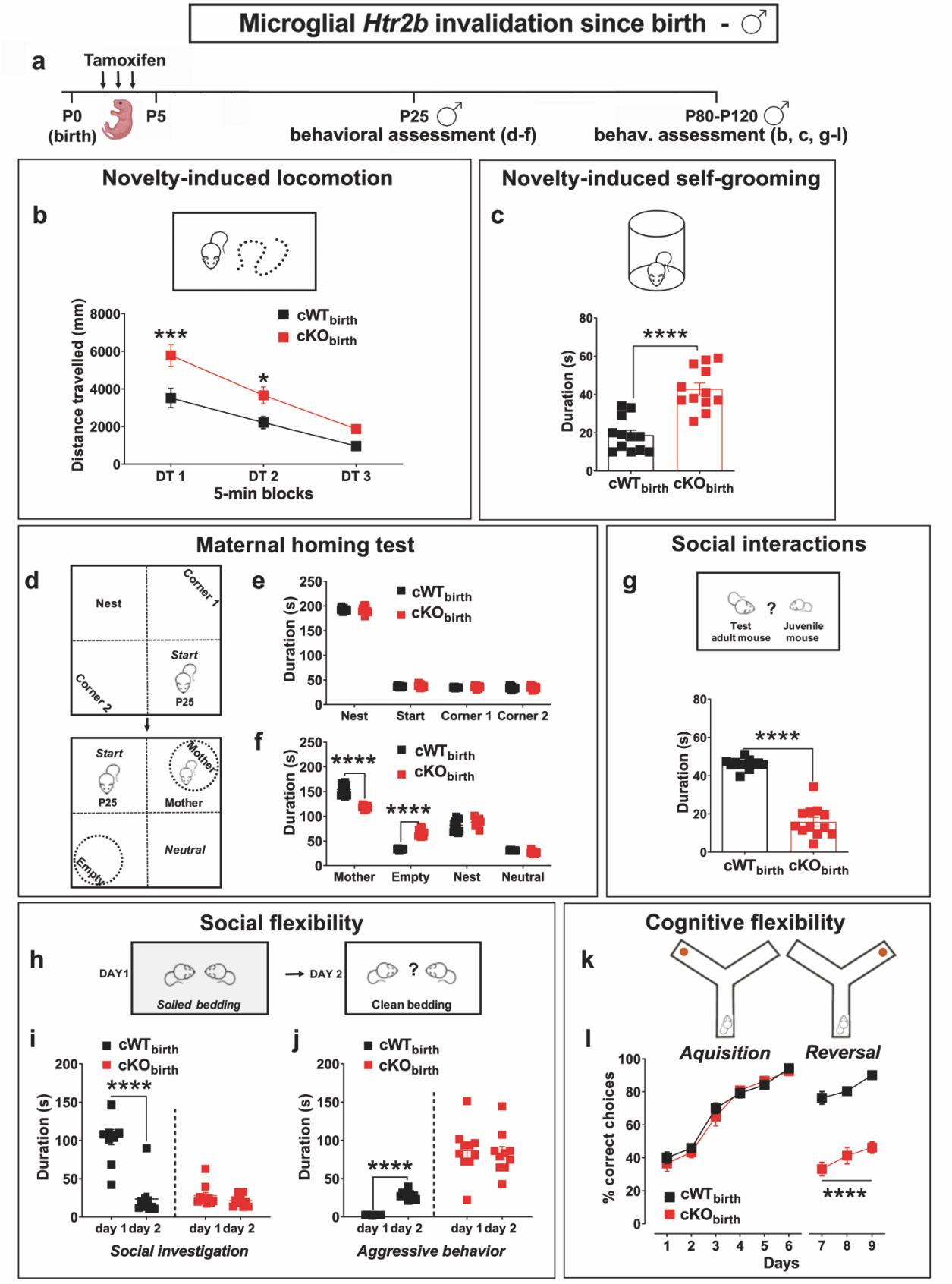
Microglial Htr2b invalidation since birth - ♂
a
Tamoxifen
P0 (birth)
P5
P25 ♂ behavioral assessment (d-f)
P80-P120 ♂ behav. assessment (b, c, g-l)
Novelty-induced locomotion
b
Distance travelled (mm)
cWT birth
cKO birth
DT 1
DT 2
DT 3
5-min blocks
Novelty-induced self-grooming
c
Duration (s)
Maternal homing test
d
Nest
Corner 1
Start
Corner 2
P25
Mother
Neutral
Empty
e
Nest
Start
Corner 1
Corner 2
f
Mother
Empty
Nest
Neutral
Social interactions
g
Test adult mouse
Juvenile mouse
Social flexibility
h
DAY1
Soiled bedding
DAY 2
Clean bedding
i
Social investigation
j
Aggressive behavior
day 1 day 2
Cognitive flexibility
k
l
Aquisition
Reversal
% correct choices
Days

Fig. 3 | Absence of 5-HT$_{2B}$ receptors in microglia since birth impacts activity in a novel environment, sociability and flexibility in male mice. a, Timeline of tamoxifen treatment for early microglial *Htr2b* invalidation, and the behavioral tests performed in juvenile (maternal homing test) or adult male mice. **b**, Distance travelled (DT) by male mice placed in a novel environment in 5-min blocks (DT1, 2, 3) (n = 12 male mice/genotype, two-way RM-ANOVA: significant main effect of DT P < 0.0001, F2,44 = 69.85 and genotype P = 0.0040, F1,22 = 10.36); note that the increased locomotion is significant only in the first 10 min of test (Sidak multiple comparisons: cWT$_{birth}$ vs. cKO$_{birth}$, DT1, p = 0.0006; DT2, p = 0.0416). **c**, The time spent self-grooming when male mice are placed in an unknown cylindrical arena is strongly enhanced in cKO$_{birth}$ compared to cWT$_{birth}$ adult male mice (n = 12 male mice/genotype, unpaired t-test, p < 0.0001). **(d-f)** Maternal homing test at P25, n = 12 male mice/genotype**. d**, Scheme of maternal homing test: habituation (upper panel) and test (lower panel). **e,** Similar behavior of cWT$_{birth}$ and cKO$_{birth}$ mice during the habituation period. **f**, Time spent in each corner during the homing test (two-way RM-ANOVA: significant main effects of interaction $P < 0.0001$, $F_{3,66} = 77.11$, zone $P < 0.0001$, $F_{3,66} = 847.0$ and genotype $P = 0.0004$, $F_{1,22} = 17.74$); note that with cKO$_{birth}$ mice, the time spent in the mother corner is strongly reduced (Sidak multiple comparisons: mother corner, cWT$_{birth}$ vs. cKO$_{birth}$, p < 0.0001), at the benefit of the empty corner (Sidak multiple comparisons: empty corner, cWT$_{birth}$ vs. cKO$_{birth}$, p < 0.0001). **g**, The time spent interacting with an unfamiliar juvenile in a neutral territory is strongly reduced in cKO$_{birth}$ adult male mice compared to cWT$_{birth}$ (n = 12 male mice/genotype, unpaired t-test, p < 0.0001). (**h-j)**, Assessment of social flexibility, n = 10 male mice/genotype**. h**, Scheme of the approach used to assess spontaneous social behavior in the home cage and social flexibility of males, using the change of litter bedding on day 2 as an environmental challenge. **i**, Duration of social investigation, before (day 1) and after (day 2) litter bedding change; note that only cWT$_{birth}$ mice modified their behavior in agreement to the change in social hierarchy induced by environmental challenge, showing less social investigation on day 2 (two-way RM-ANOVA: significant main effects of interaction $P < 0.0001$, $F_{1,18} = 64.13$; day $P < 0.0001$, $F_{1,18} = 87.52$ and genotype $P = 0.0098$, $F_{1,18} = 22.76$; Sidak multiple comparisons: cWT$_{birth}$, day 1 vs. day 2, p < 0.0001). **j**, Duration of aggressive behavior before (day 1) and after (day 2) litter bedding change; note that on day 2, only cWT$_{birth}$ mice showed an increased aggressive behavior compared to day 1 (two-way RM-ANOVA: significant main effects of interaction $P < 0.0001$, $F_{1,18} = 68.52$; day $P < 0.0001$, $F_{1,18} = 40.81$ and genotype $P < 0.0001$, $F_{1,18} = 55.91$; Sidak multiple comparisons: cWT$_{birth}$, day 1 vs. day 2, p < 0.0001). (**k-l)**, Assessment of cognitive flexibility, n = 12 male mice/genotype. **k**, Scheme of the Y-maze reversal learning task. In the acquisition phase, male mice were trained to find the food reward in one arm of the Y-maze. In the reversal procedure, the reward location was switched to the other arm. **l**, During the acquisition phase, all mice reached the criterion to choose the correct arm of the Y-maze; however, cKO$_{birth}$ male mice failed to perform the reversal phase of the test (two-way RM-ANOVA: significant main effects of phase $P = 0.0001$, $F_{2,44} = 11.28$ and genotype $P < 0.0001$, $F_{1,22} = 138.0$); Sidak multiple comparisons: cWT$_{birth}$ vs. cKO$_{birth}$, day 7, p < 0.0001; day 8, p < 0.0001; day 9, p < 0.0001. All graphs show mean±s.e.m. and points in (**c, e-g, i, and j**) represent individual animals. *p < 0.05, ***p < 0.005, ****p < 0.0001.

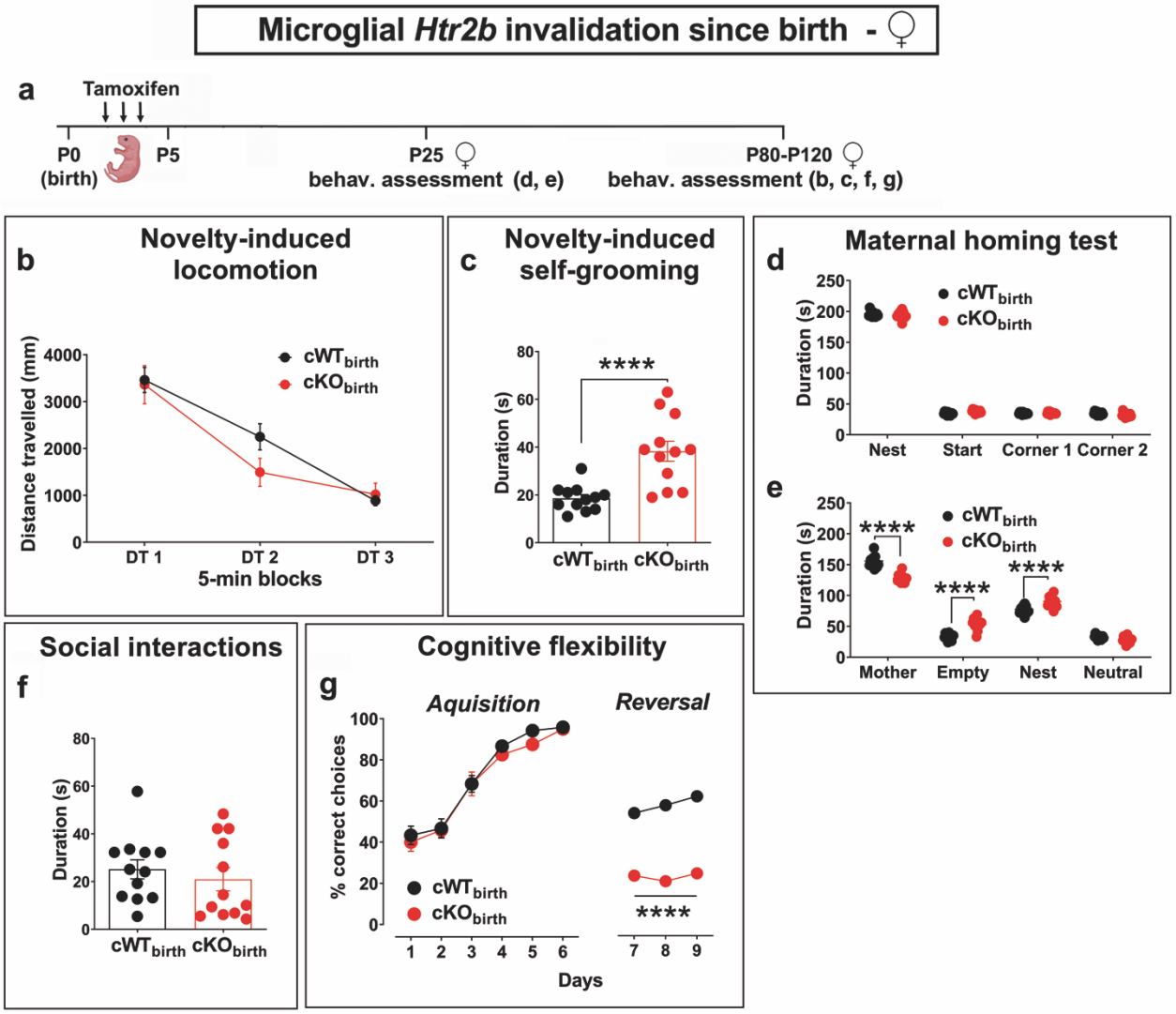

Fig. 4 | Absence of 5-HT$_{2B}$ receptors in microglia since birth impacts activity in a novel environment, sociability and flexibility in female mice. a, Timeline of tamoxifen treatment for early microglial *Htr2b* invalidation, and the behavioral tests performed in juvenile (maternal homing test) or adult female mice. (**b-g**), Behavioral assessment in cWT$_{birth}$ and cKO$_{birth}$ female mice, n = 12 female mice/genotype. **b**, Distance travelled by female mice placed in a novel environment in 5-min blocks (DT1, 2, 3) (two-way RM-ANOVA: significant main effect of DT $P < 0.0001$, $F_{2,44}) = 84.07$). **c**, The time spent grooming in response to a novel environment is strongly enhanced in cKO$_{birth}$ adult female mice compared to cWT$_{birth}$ (unpaired t-test, $p < 0.0001$). **d**, In the habituation phase of the maternal homing test, cWT$_{birth}$ and cKO$_{birth}$ P25 female mice displayed similar behavior, with a strong preference for the nest corner. **e**, In the test phase however, the time spent in each corner differed between cWT$_{birth}$ and cKO$_{birth}$ P25 female mice (two-way RM-ANOVA: significant main effects of interaction $P < 0.0001$, $F_{3,66} = 41.29$ and zone $P < 0.0001$, $F_{3,66} = 933.1$); note that the preference for the mother corner was strongly reduced in cKO$_{birth}$ compared to cWT$_{birth}$ mice (Sidak multiple comparisons: mother corner, cWT$_{birth}$ vs. cKO$_{birth}$, $p < 0.0001$), at the benefit of the time spent in the empty and nest corners (Sidak multiple comparisons: empty corner, cWT$_{birth}$ vs. cKO$_{birth}$, $p < 0.0001$; nest corner, cWT$_{birth}$ vs. cKO$_{birth}$, $p < 0.0001$). **f**, Duration of interaction with a juvenile conspecific in a neutral territory is similar in cWT$_{birth}$ and

cKO_{birth} adult female mice. **g**, In the reversal learning test to assess cognitive flexibility, cWT_{birth} and cKO_{birth} female mice similarly reached the acquisition criterion; however, cKO_{birth} female mice failed to perform the reversal phase of the test (two-way RM-ANOVA: significant main effects of interaction $P = 0.0068$, $F_{2,44} = 5.607$; phase $P = 0.0004$, $F_{2,44} = 9.250$ and genotype $P < 0.0001$, $F_{1,22} = 427.3$; Sidak multiple comparisons: cWT_{birth} vs. cKO_{birth}, day 7, $p < 0.0001$; day 8, $p < 0.0001$; day 9, $p < 0.0001$). All graphs show mean±s.e.m. and points in (**c-f**) represent individual animals. ****$p < 0.0001$.

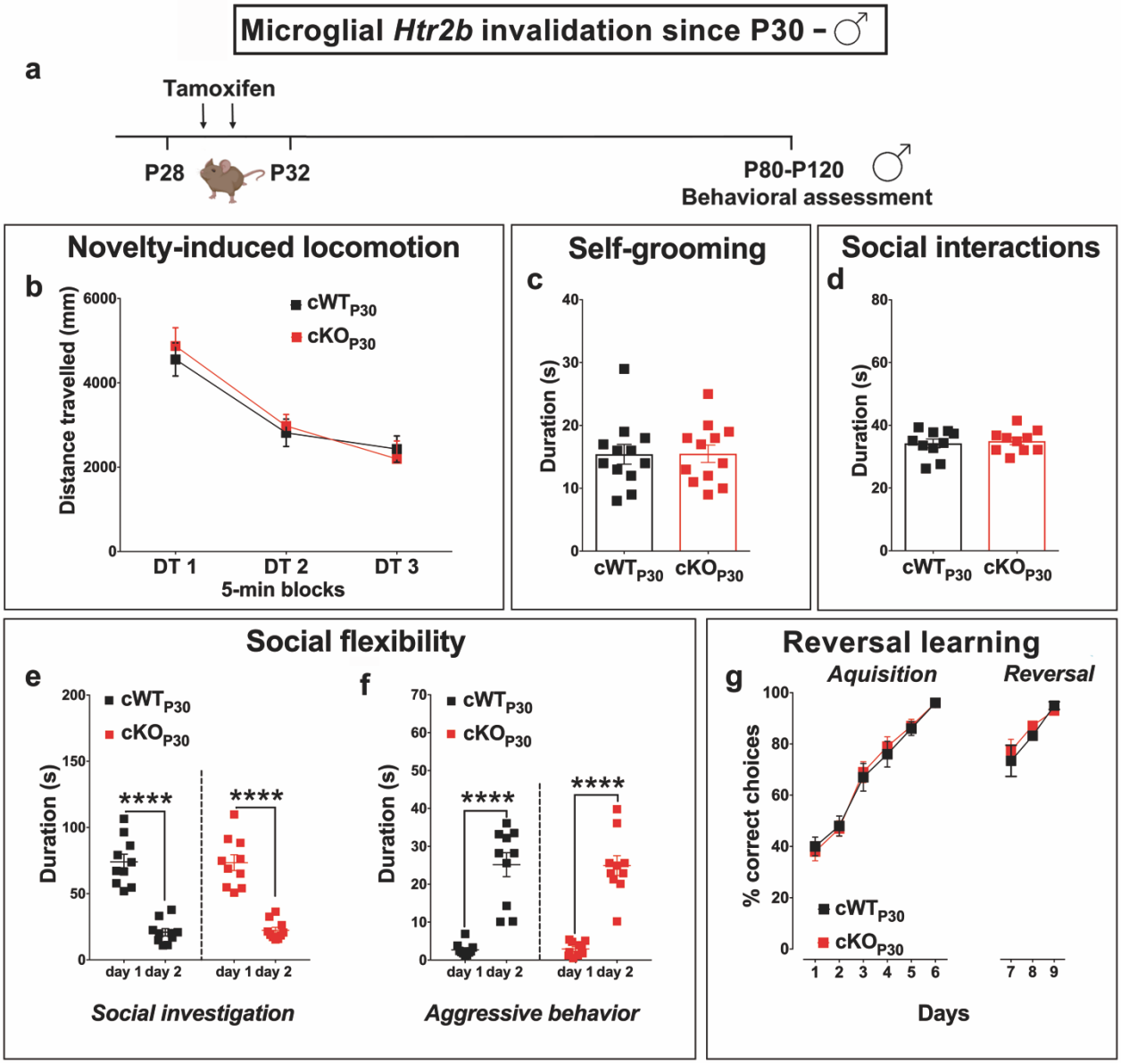

Fig. 5 | Ablation of 5-HT$_{2B}$ receptors in microglia at P30 does not alter spontaneous behaviors in adult male mice. a, Timeline of tamoxifen treatment for late microglial *Htr2b* invalidation (P28-32), and the behavioral tests performed in adult male mice. **b**, Similar distance travelled in response to a novel environment in 5-min blocks (DT) (n = 10 male mice/genotype, two-way RM-ANOVA: significant main effect of DT $P < 0.0001$, $F_{2,36} = 70.78$). **c**, Similar time spent self-grooming in response to a novel environment in cWT$_{P30}$ and cKO$_{P30}$ adult male mice (n = 12 male mice/genotype). **d**, Similar time spent interacting with a juvenile conspecific in a neutral territory in cWT$_{P30}$ and cKO$_{P30}$ adult male mice (n = 10 male mice/genotype). **(e-f)**, Similar social flexibility of cWT$_{P30}$ and cKO$_{P30}$ adult male mice, in response to a challenge of social hierarchy induced by the change of litter bedding on day 2 (n = 10 adult male mice/genotype). **e**, The change of litter bedding on day 2 induced a decrease in the time spent in social investigation in both genotypes (two-way RM-ANOVA: significant main effect of day $P < 0.0001$, $F_{1,18} = 203.7$; Sidak multiple comparisons: cWT$_{P30}$, day 1 vs. day 2, $p < 0.0001$; cKO$_{P30}$, day 1 vs. day 2, $p < 0.0001$). **f,** The change of litter bedding on day 2 induced an increase in the time spent in aggressive behavior in

both genotypes (two-way RM-ANOVA: significant main effect of day $P < 0.0001$, $F_{1,18} = 145.8$; Sidak multiple comparisons: cWT_{P30}, day 1 vs. day 2, $p < 0.0001$; cKO_{P30}, day 1 vs. day 2, $p < 0.0001$). **g**, Y-maze reversal learning test shows no difference in cognitive flexibility task in cWT_{P30} and cKO_{P30} adult male mice (*n* = 10 male mice/genotype). All graphs show mean±s.e.m. and points in (**c-f**) represent individual animals. ****p < 0.0001.

Supplementary material

Fig S1
Fig S2
Fig S3 with methods
Fig S4
Fig S5

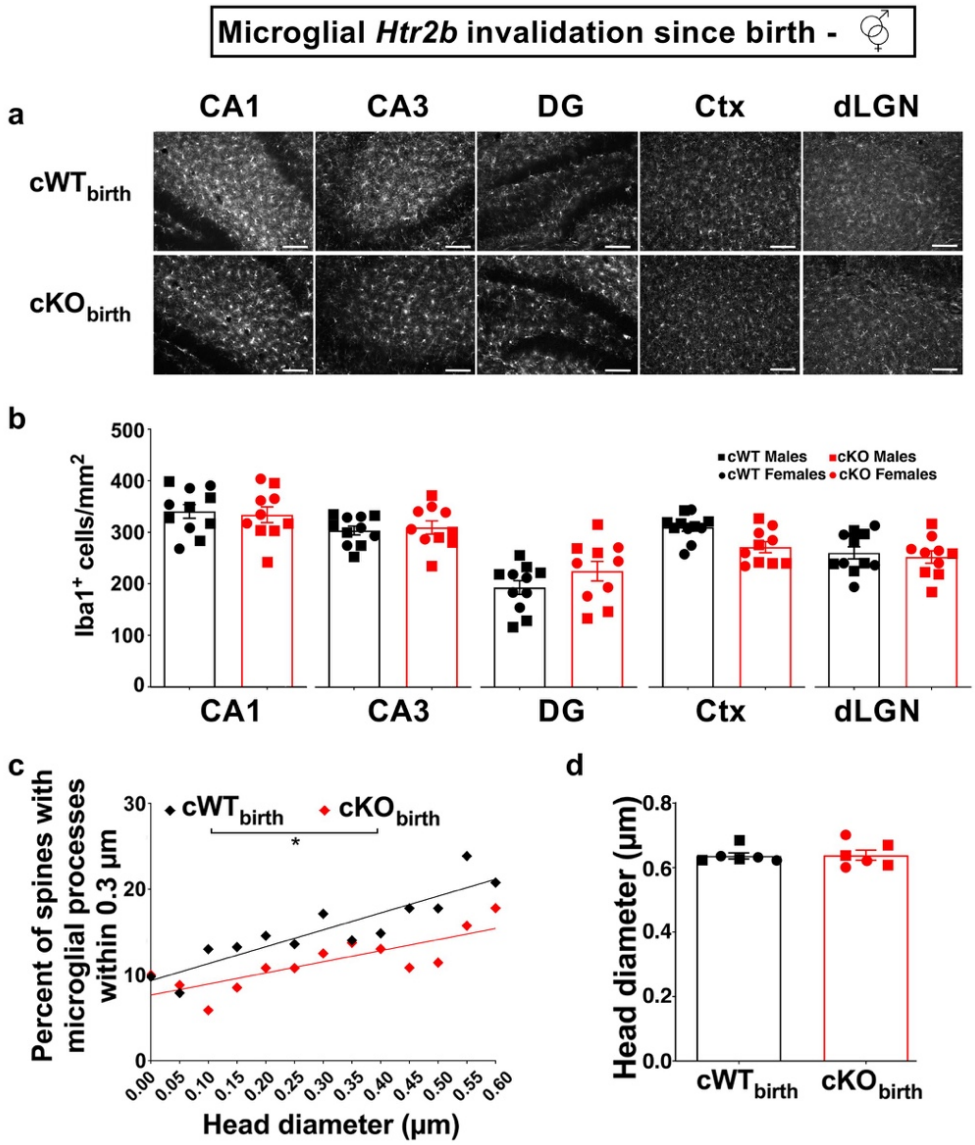

Fig. S1 | Early invalidation of *Htr2b* in microglia does not affect microglial density but decreases the percent of spines with microglial processes in proximity, independently of their head diameter. a, Representative images of Iba1$^+$ cells on 20x images collected in CA1, CA3 and dentate gyrus (DG) of the dorsal hippocampus, retrosplenial cortex (Ctx) and dorsal lateral geniculate nucleus of the thalamus (dLGN) in cWT$_{birth}$ and cKO$_{birth}$ mice at P15. Scale bars: 100 µm. **b**, Densities of Iba1$^+$ cells are similar in cWT$_{birth}$ (black, *n* = 11 mice) and cKO$_{birth}$ (red, *n* = 10 mice) mice at P15. **c**, Absence of 5-HT signal in microglia since birth is associated to reduced percent of spines with microglial processes within 0.3 µm at P15, independently of the protrusion head diameter (cWT$_{birth}$ mice, *n* = 13 mice; cKO$_{birth}$ mice, *n* = 12 mice; Kolmogorov-Smirnov test, P = 0.0461). **d**, Similar average head diameter of protrusions on secondary apical dendrites of CA1 pyramidal neurons in cWT$_{birth}$ and cKO$_{birth}$ mice at P15. *n* = 6 mice/genotype, average of 30 dendrites per mouse. Graphs in (**c**) show mean±s.e.m. and points in (**b, d**) represent individual animals. These analyses were performed on mixed males and females. *p < 0.05. Square symbols: males; round: females; diamond: mixed.

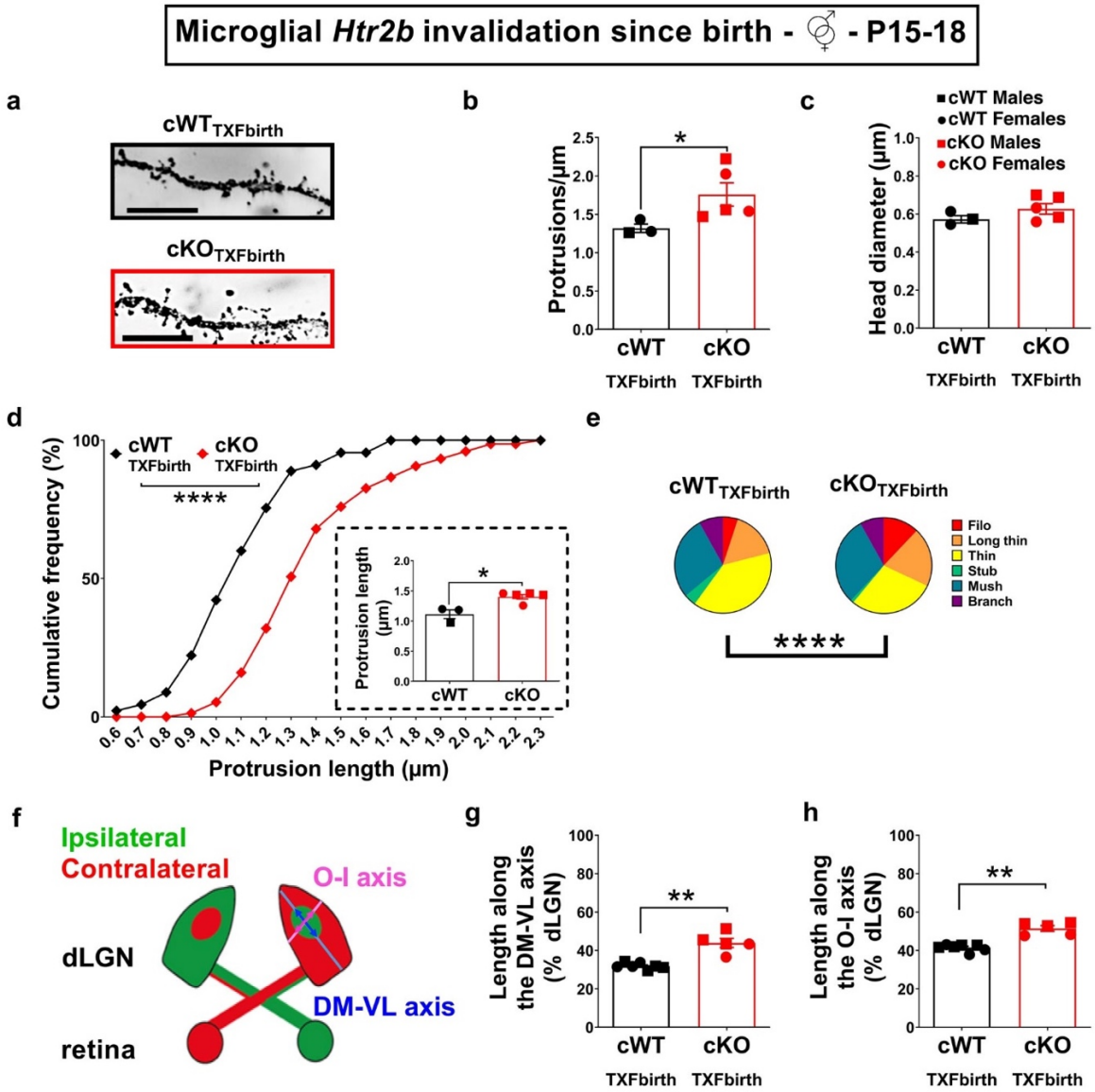

Fig. S2 | Early invalidation of *Htr2b* in microglia impacts on the maturation of cortical spines and of the dLGN. (a-e) Analysis of dendritic protrusions of L2/L3 cortical principal neurons in cWT_{birth} and cKO_{birth} mice at P15 (average of 15 dendrites per mouse; cWT_{birth}, *n* = 3 mice; cKO_{birth}, *n* = 5 mice; mixed males and females). **a**, Representative images of apical secondary dendrites of L2/L3 cortical principal neurons labeled with Golgi staining, scale bar: 10 µm. **b**, Quantification of protrusion density on secondary apical dendrites of L2/L3 principal neurons, which shows a significant increase in protrusion density in cKO_{birth} mice (Mann-Whitney test, p = 0.0357). **c**, Similar average head diameter of protrusions on secondary apical dendrites of L2/L3 principal neurons in cWT_{birth} and cKO_{birth} mice. **d**, Cumulative distribution plot for the average length of protrusions on secondary apical dendrites of L2/L3 principal neurons in cWT_{birth} and cKO_{birth} mice; note the significant rightward shift in cKO_{birth} as compared to cWT_{birth} mice (cWT_{birth}, *n* = 45 dendrites from 3 mice; cKO_{birth}, *n* = 75 dendrites from 5 mice; Kolmogorov-Smirnov test, p < 0.0001). In the inset, quantification of protrusion length obtained averaging 15 dendrites/mouse, which confirms a significant increase in average protrusion length in cKO_{birth} mice (Mann-Whitney test, p = 0.0357). **e**, Pie

charts showing the altered distribution of protrusion types in the cortex of cKO_{birth} as compared to cWT_{birth} mice at P15 (cWT_{birth}, *n* = 45 dendrites from 3 mice; cKO_{birth}, *n* = 75 dendrites from 5 mice; Chi-square test, $p < 0.0001$). **(f-h)**, Extension of the ipsilateral retinal projections into the dLGN, in cWT_{birth} and cKO_{birth} mice at P17-18 (cWT_{birth}, *n* = 7 mice; cKO_{birth}, *n* = 5 mice; mixed males and females). **f**, Diagram of the dLGN showing the outer-inner (O-I) and dorsomedial-ventrolateral (DM-VL) axes. The lengths of the ipsilateral patch along the DM-VL axis (dark blue arrow) and the O-I axis (dark pink arrow) were divided by the lengths of the dLGN along the DM-VL axis (light blue line) and the O-I axis (light pink line), respectively. **g**, In cKO_{birth} mice, ipsilateral retinal projections cover more territory along the DM-VL axis than in cWT_{birth} mice (Mann-Whitney test, $p = 0.0025$). **h**, In cKO_{birth} mice, ipsilateral retinal projections cover more territory along the O-I axis than in cWT_{birth} mice (Mann-Whitney test, $p = 0.0025$). All graphs (except cumulative curve in **d**, and pie chart in **e**) show mean±s.e.m. and points in (**b-c**, inset of **d**, and **g-h**) represent individual animals. *$p < 0.05$, **$p < 0.01$, ****$p < 0.0001$. Square symbols: males; round: females; diamond: mixed.

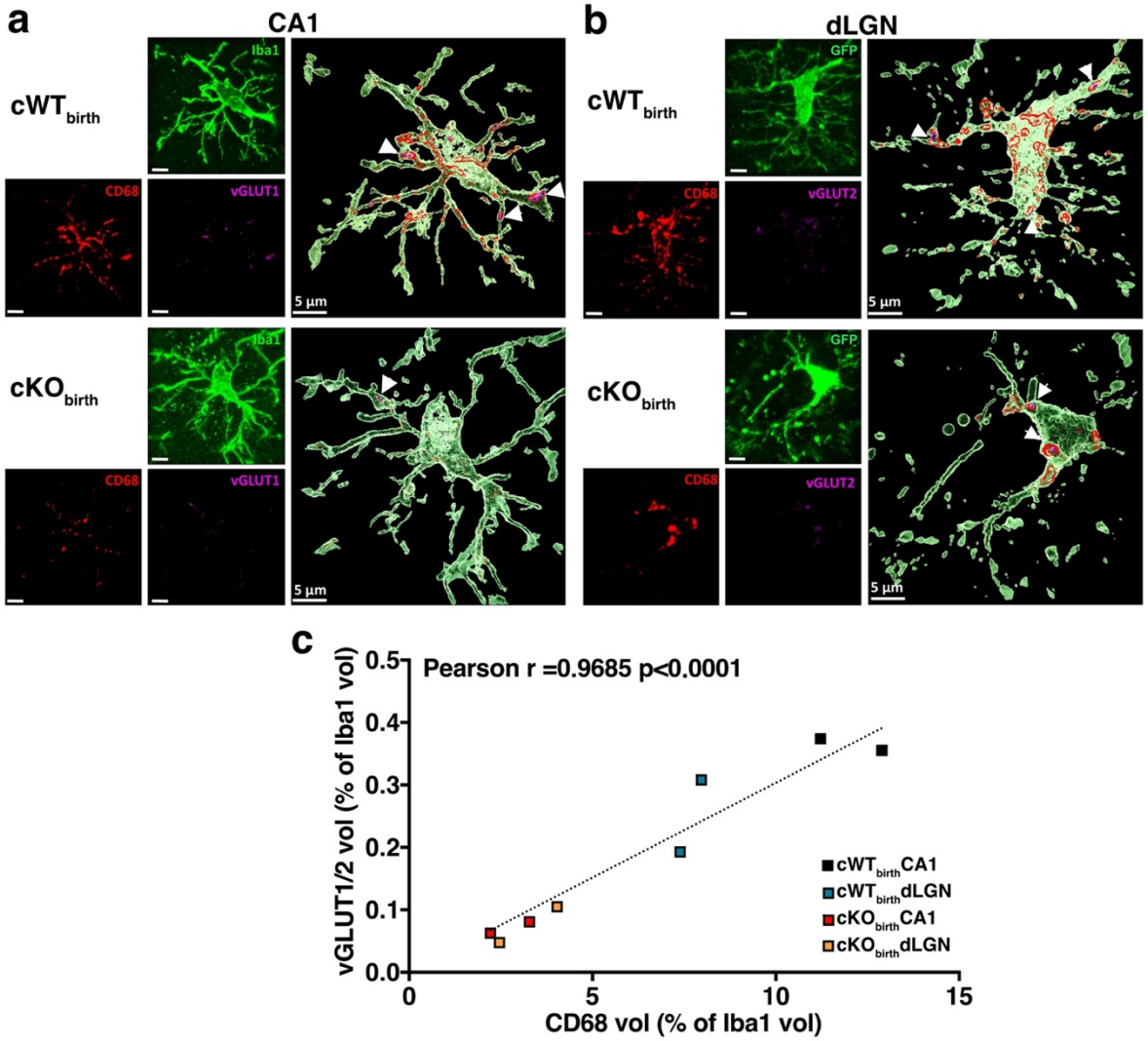

Fig. S3 | Microglia in the hippocampus and dLGN of the thalamus contain presynaptic material at P15. **a-b**, Representative images of microglia in CA1 (**a**) and dLGN (**b**) of cWT_{birth} and cKO_{birth} P15 mice. Left panels: immunostainings with anti-Iba1 or anti-GFP (green, **a** and **b,** respectively) to delineate the volume of microglia, with anti-CD68 (red) to locate their lysosomal compartment (i.e. only $CD68^+$ pixels within the Iba1 staining are shown) and with anti-vGLUT1 or vGLUT2 (purple, **a** and **b,** respectively) to identify presynaptic material within lysosomes (i.e. only $vGLUT^+$ pixels within the CD68 staining are shown). Right panels: 3D reconstruction and overlay of $Iba1^+$ volumes, $CD68^+$ lysosomes and vGLUT clusters. The arrows indicate clusters of vGLUT within microglial lysosomes. **c**, the volume of vGLUT material within microglia is proportional to the volume of the microglial phagolysosomal (i.e., $CD68^+$) compartment (Pearson coefficient r=0.9685, p<0.0001). It is also visible on this graph that microglia of cKO_{birth} P15 animals have reduced CD68 and vGLUT staining compared to cWT_{birth}, no matter the brain region. Symbols represent individual animals.

Supplementary Methods for Fig. S3 - Antibodies: to colocalize vGLUT1 in the CA1, we used the combination of Rabbit anti-Iba1, Rat anti-CD68 and Guinea-pig anti-vGLUT1 (0.002 µg/µL, 1/500,

Synaptic System 135304) revealed by Donkey anti-Rabbit 488, Donkey anti-Rat Cy3 and Donkey anti-Guinea pig AlexaFluor647 (1:500, Jackson Laboratories 706-605-148); **b,** to colocalize vGLUT2 in the dLGN, we used the combination of Chicken anti-GFP (1/500, Invitrogen, A10262) to reveal microglia (which express YFP together with Cre recombinase, although at a undetectable level without amplification), Rat anti-CD68 and Rabbit anti-vGLUT2 (1/500, homemade[75], gift of Veronique Fabre), revealed with Donkey anti-Chicken Alexa Fluor488 (1:500, Jackson Laboratories, 703-545-155), Donkey anti-Rat Cy3 and Donkey anti-Rabbit AlexaFluor405 (1:500, Abcam, Ab175651). *Rabbit anti-Iba1, Rat anti-CD68, Donkey anti-Rabbit 488 and Donkey anti-Rat Cy3: same references and concentrations than in the main Methods.*

75. Herzog, E., Bellenchi, G.C., Gras, C., Bernard, V., Ravassard, P., Bedet, C. *et al.* The Existence of a Second Vesicular Glutamate Transporter Specifies Subpopulations of Glutamatergic Neurons. *J. Neurosci.* **21**, RC181–RC181 (2001). DOI: https://doi-org.proxy.insermbiblio.inist.fr/10.1523/JNEUROSCI.21-22-j0001.2001

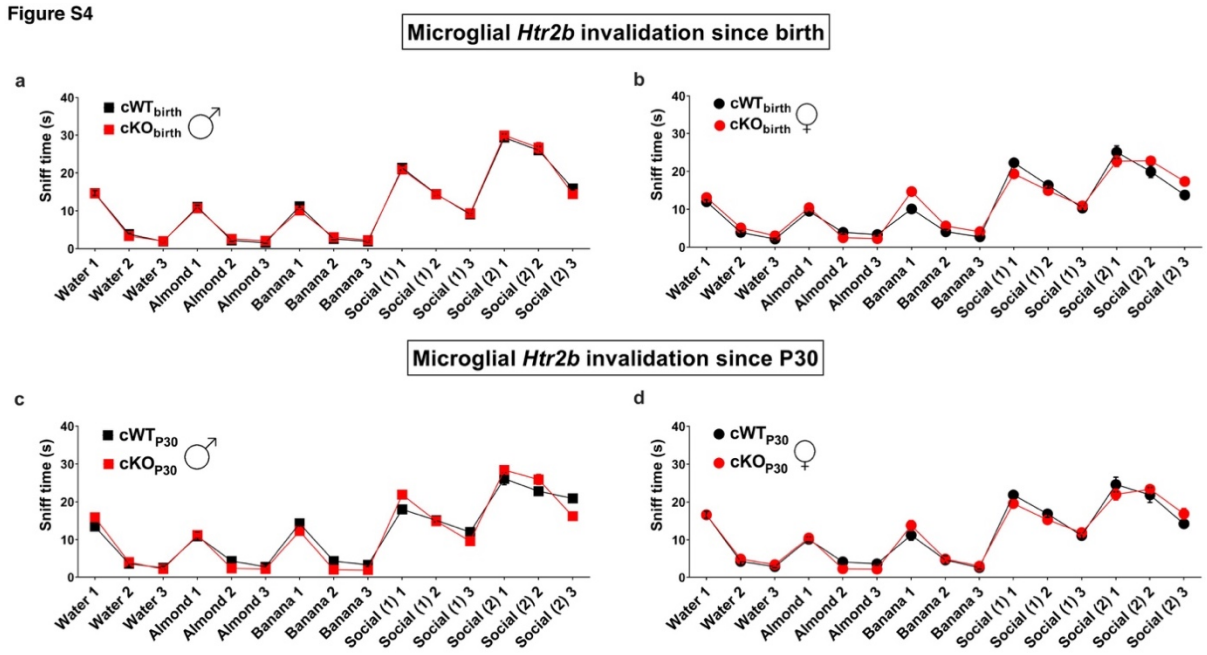

Fig. S4 | Early and late invalidations of *Htr2b* in microglia do not affect olfaction in mice. Olfactory habituation/dishabituation is identical in cWT_{birth} and cKO_{birth} mice invalidated for the 5-HT_{2B} receptors since birth (**a**, males, 12 male mice/genotype; **b**, females, 12 female mice/genotype) and since P30 (**c**, males, 10 male mice/genotype; **d**, females, n = 10 cWT_{P30} and n = 8 cKO_{P30} female mice). All graphs show mean±s.e.m.

Figure S5

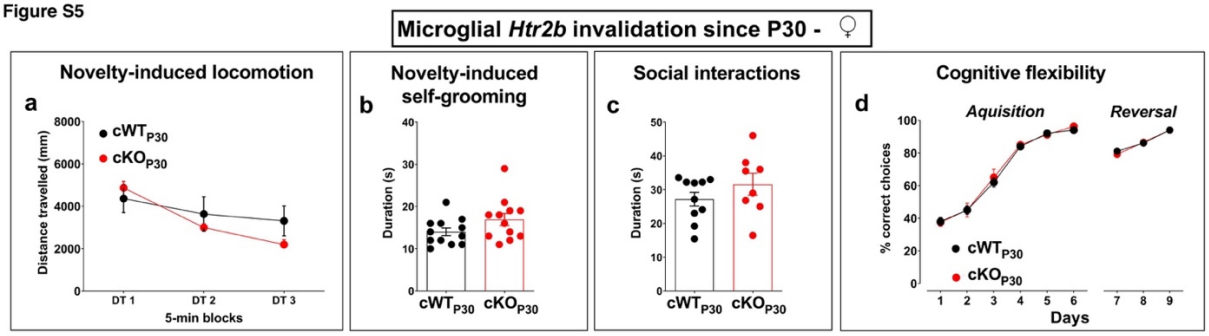

Fig. S5 | Late ($_{P30}$) invalidation of microglial 5-HT$_{2B}$ receptors does not affect activity in a novel environment, sociability nor flexibility in adult female mice.

a, Similar distance travelled in response to a novel environment in 5-min blocks (DT) (n = 10 cWT$_{P30}$ and n = 8 cKO$_{P30}$ female mice; two-way RM-ANOVA: significant main effect of DT $P < 0.0001$, $F_{2,36} = 70.78$). **b**, Similar time spent self-grooming in response to a novel environment in cWT$_{P30}$ and cKO$_{P30}$ adult female mice (n = 12 mice/genotype). **c**, Similar time spent interacting with a juvenile conspecific in a neutral territory in cWT$_{P30}$ and cKO$_{P30}$ adult female mice (n = 10 cWT$_{P30}$ and n = 8 cKO$_{P30}$ mice). **d**, Y-maze reversal learning shows no difference in cognitive flexibility task in cWT$_{P30}$ and cKO$_{P30}$ adult female mice (n = 10 cWT$_{P30}$ and n = 8 cKO$_{P30}$ mice). All graphs show mean±s.e.m. and points in (**b, c**) represent individual animals.